



BSc. THESIS

Optical improvement of Fourier transform
Raman spectrometers

Sami Dzsaber

Thesis advisor: Ferenc Simon
Professor
Department of Physics
Institute of Physics
BME

Budapest University of Technology and Economics

**BME
2013.**

Contents

A szakdolgozat kiírása	4
Önállósági nyilatkozat	5
Köszönetnyilvánítás	6
1 Introduction and motivation	7
2 Theoretical background	9
2.1 Theory of Raman scattering	9
2.2 General build-up of Raman spectrometers	12
2.2.1 Excitation and light collection	12
2.2.2 Fourier transform spectrometers	14
2.2.3 Sampling and the He-Ne laser	16
2.2.4 Effect of sampling parameters on intensity	18
2.2.5 Advantages of the FT technique	20
3 Experimental methods	22
3.1 Reference sample	22
3.2 The modern interference filters	24
3.3 The detectors used in FT-Raman spectroscopy	25
3.3.1 NIR photodiode	25
3.3.2 The photomultiplier tube	28
4 Results and discussion	31
4.1 Optical upgrade of a commercial FT-Raman spectrometer	31
4.1.1 Optical path and filters	31
4.2 Improvement of a microscope FT-Raman spectrometer	39
4.2.1 Original state of the apparatus	39
4.2.2 Modifying the optical path	41
4.2.3 Improvement in Raman photon collection efficiency	45
4.2.4 Application of inverse beam expander	46
4.3 Development of a visible FT-Raman spectrometer	49
4.3.1 The optical configuration of VIS FT-Raman spectrometer	49
4.3.2 Electronic configuration	50
4.3.3 The signal-to-noise performance	51
4.3.4 The signal	53
4.3.5 Quality of the spectrometer	55
5 Summary and outlook	58
A Central Limit Theorem	61
B Fourier transformation and the FFT	62
C The shot noise	65

D The interferometer and other optical parts	65
E Applied HAMAMATSU PMT datasheet	67

A szakdolgozat kiírása

Az egyfalú szén nanocsövek (SWCNT-k) rezgési tulajdonságai mind az alkalmazásaik, mind az alap kutatások szempontjából érdekesek. A vizsgálati módszerek közül kimagyul a Raman spektroszkópia, mely SWCNT-k esetén nem invazív módon, tömbi mintákról ad információt, úgy mint pl. a nanocső átmérő eloszlás és tisztaság. A BME-n rendelkezünk egy, a Bécsi Egyetemről kapott FT-Raman spektrométerrel, mely jelenleg nem működik. A berendezés üzembe helyezéséhez keresünk egy kísérletező alkatú, kitartó és precíz munkavégzésű hallgatót, aki hajlandó és tud is finom optikai beállításokkal dolgozni. A jelentkező feladatai: 1) A Raman és az FT-Raman módszerek elvének megértése és összefoglalása, 2) a BME Bruker FT-Raman berendezés beüzemelése és fejlesztése, valamint a Bécsi Egyetem hasonló spektrométerén az ún. NIR-Raman mikroszkóp optikai tulajdonságainak javítása, 3) nitrogénnel hűtött kriosztát beüzemelése, és 4) az FT-Raman spektrométer optikájának átépítése, hogy Raman méréseket tegyen lehetővé a látható, 532 nm-es gerjesztéssel szén nanocsöveken. A 4)-es pont teljes megvalósítása nem feltétlenül követelmény, mivel itt adódhatnak előre nem látott nehézségek.

Önállósági nyilatkozat

Alulírott Dzsaber Sami, a Budapesti Műszaki és Gazdaságtudományi Egyetem hallgatója kijelentem, hogy ezt a szakdolgozatot meg nem engedett segédeszközök nélkül, saját magam készítettem, és csak a megadott forrásokat használtam fel. Minden olyan szövegrészt, adatot, diagramot, ábrát, amelyet azonos értelemben más forrásból átvettem, egyértelműen, a forrás megadásával megjelöltem.

Budapest, 2013. május 29.

Dzsaber Sami

Köszönetnyilvánítás

Köszönettel tartozom témavezetőmnek Prof. Simon Ferencnek, hogy megadott minden lehetőséget és támogatást a munkám során. Az elmúlt években mindig számíthattam szakmai tudására míg ötleteimet és elképzeléseimet pozitívan fogadta. Hálás vagyok neki a jó tanácsaiért, a munkához való hozzáállása irányadó számomra.

Hálával tartozom Prof. Thomas Pichlernek, hogy lehetővé tette számomra szakmai gyakorlatomat a Bécsi Egyetemen, továbbá köszönet illeti kutatócsoportjának tagját Dr. Christian Krambergert az általa nyújtott segítségéért, mellyel munkámat és az ott töltött öt hetet gördülékennyé tette.

Köszönettel tartozom Dr. Fülöp Ferencnek az IFS66v spektrométer elektronikájának javításában nyújtott segítségéért. Továbbá köszönet illeti Dr. Kézsmárki Istvánt és kutató csoportját amiért biztosították a PMT deterktort és egyéb optikai alkatrészeket és Dr. Fehér Tituszt, hogy biztosította számomra az 532 *nm* szilárdtest lézert.

Köszönet illeti Horváth Bélát, Bacsa Sándort és Halász Tibort a műhely munkákban nyújtott segítségükért. Továbbá köszönöm Negyedi Milán és Szirmai Péter hallgató társaimnak jó tanácsaikat.

Köszönettel tartozom szüleimnek töretlen támogatásukért és bizalmukért.

Acknowledgments

I am grateful to my thesis advisor Prof. Ferenc Simon for ensuring every opportunity and support for my work. During the last years I would always count for his professional knowledge, while my opinion and conceptions always met his welcoming attitude. I thank him for his supporting advises, his attitude for work is exemplary for me.

I gratefully acknowledge the hospitality of Prof. Thomas Pichler at the University of Vienna and that of his group, particularly the help of Dr. Christian Kramberger, during my five week long stay therein.

I thank Dr. Ferenc Fülöp for repairing some of the electronics of IFS66v spectrometer. Dr. István Kézsmárki and his group is acknowledged for letting us use the PMT and some smaller optical instruments and also is Dr. Titus Fehér for letting us use his 532 *nm* solid-state laser.

I Thank Béla Horváth, Sándor Bacsa and Tibor Halász for their for providing the mechanical parts. I also like to thank my fellow students Milan Negyedi and Péter Szirmai for their advises.

Financial support by the European Research Council Grant Nr. ERC-259374-Sylo is acknowledged.

1 Introduction and motivation

Raman spectroscopy together with other optical spectroscopy methods is a powerful non-invasive analytic tool, widely used in physics, chemistry and biology. Raman spectroscopy is an essentially low light methodology which relies on how well unwanted light sources can be suppressed. In recent years, Raman spectroscopy has been revolutionized by the wide-spread use of high quality interference filters, which provide very short transition ranges between 6-7 orders of magnitude transmission changes. The present thesis was motivated by this advance to improve the optical layout of FT-Raman spectrometers with the use of interference filters.

This thesis presents the results of three projects; the first was the optical upgrade of a *Bruker IFS66V* Fourier transform infrared (FT-IR) Raman spectrometer that was received as a gift from the University of Vienna. The upgrade was available due to the introduction of modern interference filters and by simplifying the optical path of the Raman beam, by means of reducing the number of optical elements.

The second was the upgrade of the confocal NIR Raman microscope system at the University of Vienna by means of building a high throughput optical coupling between the interferometer and the Raman microscope. In the *Electronic Structure of Materials group* (University of Vienna) a *Nikon Eclipse E400* microscope was coupled to a *Bruker RFS100/S* Raman spectrometer. There were two major problems to solve first, there were substantial losses in the laser intensity while reaching the sample: due to the complicated optical path, and the great number of the optical parts ,and also due to the the inferior quality of the built-in Bruker laser clean up filter, which has about 50% transmission, the whole laser throughput of the system was 18% . Improving the laser throughput of the system is important when used for annealing, and it also extends the lifetime of the laser as it can be operated with lower current for the same intensity on the sample. The second problem was to improve the Raman collection efficiency as it provides better Signal to Noise Ratio(SNR).

The third project was a complete rebuilding of the *Bruker IFS66V* spectrometer to operate in the visible regime, by reinstalling the excitation, collection, optical guiding and detector systems. Rebuilding the FT-Raman spectrometer, which operates in the near infrared (NIR), is seemingly just a matter of changing the optical elements from NIR to VIS types. However, fundamental differences are present for the two wavelengths as far as the detection principle is concerned. The basic technology for FT-spectroscopy was already available in the early 1980's, but it was generally considered that FT technique would yield no advantage over dispersive ones, as the multiplex advantage would be compensated by the fact that noise corresponding to the power of the detected light would be detected and spread through the whole spectrum (noise multiplex). In 1986, Hirshfeld and his colleagues showed that in case of NIR excitation, FT technique is superior to the dispersive [1], but in the case of visible excitation, where measurement is shot noise limited, it is still believed that FT technique is inadequate for acquiring Raman spectra.

In chapter 2. I discuss the theoretical background of the Raman scattering, and the

basic build-up of Raman spectrometers. In chapter 3. I discuss the method of monitoring and characterizing a Raman spectrometer, by explaining the methods of determining the signal to noise ratio. Chapter 4. provides documentation and discussion of the results; chapter 4.1. summarizes the optical upgrade of a NIR FT-Raman spectrometer (1st. project). Chapter 4.2 discusses the project number two, while chapter 4.3 discusses the built VIS FT-Raman spectrometer (3rd. project).

2 Theoretical background

2.1 Theory of Raman scattering

The basic physical phenomenon behind optical spectroscopy is the interaction of light and matter. A light quantum interacts with matter in basically two ways, either it is absorbed by a molecule, exciting it to a higher energy state, or it can scatter on it revealing the dynamics of the molecule. Raman spectroscopy is based on the latter phenomenon, and typically the scattering of monochromatic radiation is studied.

Raman scattering occurs when a photon interacts with a vibrating molecule. When a material is placed in an electric field, it will be polarized, where the degree of the polarization depends on the amplitude of the electric field, typically the dependence is linear and anisotropic which is expressed by the $\underline{\alpha}$ polarisability tensor. As for a single molecule a \underline{p} dipole momentum will be formed due to the electric field \underline{E} which is expressed by the following formula:

$$(\underline{p})_j = \sum_i \alpha_{ij} E_i \iff \underline{p} = \underline{\alpha} \underline{E} \quad (1)$$

Now suppose a diatomic molecule is vibrating with ω_m angular frequency around its equilibrium point, where the displacement time dependence is $q(t) = Q \cos \omega_m t$. The polarisability tensor depends on the spatial parameters of the molecule; in this case the distance of the atoms from the equilibrium point, that is $\alpha_{ij} = \alpha_{ij}(q)$. Now if the amplitude of the motion is small (which is the case if we consider the motion of atoms is harmonic), we can expand $\alpha_{ij}(q)$ in terms of q :

$$\alpha_{ij} = (\alpha_{ij})_0 + \frac{\partial \alpha_{ij}}{\partial q} q \quad \text{that is } \underline{\alpha} = \underline{\alpha}_0 + \underline{\alpha}_d q \quad (2)$$

This is called the electric harmonic approximation where $\underline{\alpha}_d$ is the derived tensor.

Suppose the vibrating molecule interacts with a photon, that has an electric field component $\underline{E}(t) = \underline{E}_0 \cos \omega_i t$, if we substitute this form and the form of $q(t)$ into Eq.1:

$$\underline{p} = \underline{\alpha}_0 \underline{E}_0 \cos \omega_i t + \underline{\alpha}_d \underline{E}_0 Q \cos \omega_j t \cos \omega_i t \quad (3)$$

The product of the two cosines in the last term of Eq.3 can be reduced to a sum of two cosines with the frequency of $(\omega_i + \omega_j)$ and $(\omega_i - \omega_j)$ using trigonometric identities, that reads :

$$\begin{aligned} \underline{p} &= \underline{\alpha}_0 \underline{E}_0 \cos \omega_i t + \frac{1}{2} \underline{\alpha}_d \underline{E}_0 Q \cos (\omega_i + \omega_j) t + \frac{1}{2} \underline{\alpha}_d \underline{E}_0 Q \cos (\omega_i - \omega_j) t \\ \underline{p} &= \underline{p}(\omega_i t) + \underline{p}((\omega_i + \omega_j) t) + \underline{p}((\omega_i - \omega_j) t) \end{aligned} \quad (4)$$

What we obtain is the superposition of three dipole momentum oscillating with three different frequencies.

It is a well known fact that an oscillating dipole radiates electromagnetic waves with the frequency of the oscillation:

1. the first term $\underline{p}(\omega_i t)$ oscillates with ω_i i.e. with the angular frequency of the incident electromagnetic wave, this corresponds to the elastic scattering of photon as the energy of the incident photon is conserved, this is also called *Rayleigh scattering*.
2. the second term $\underline{p}((\omega_i + \omega_j)t)$ oscillates with the sum of the photon ω_i and vibration ω_j angular frequency: the scattered photon has a higher energy of $\hbar\omega_j$ and the vibration mode is destroyed. This is called *anti-Stokes Raman scattering*.
3. the third term $\underline{p}((\omega_i - \omega_j)t)$ oscillates with the difference of the photon ω_i and vibration ω_j angular frequency: the scattered photon has less energy than the incident one giving rise to a molecule vibration mode of ω_j angular frequency. This is called *Stokes Raman scattering*

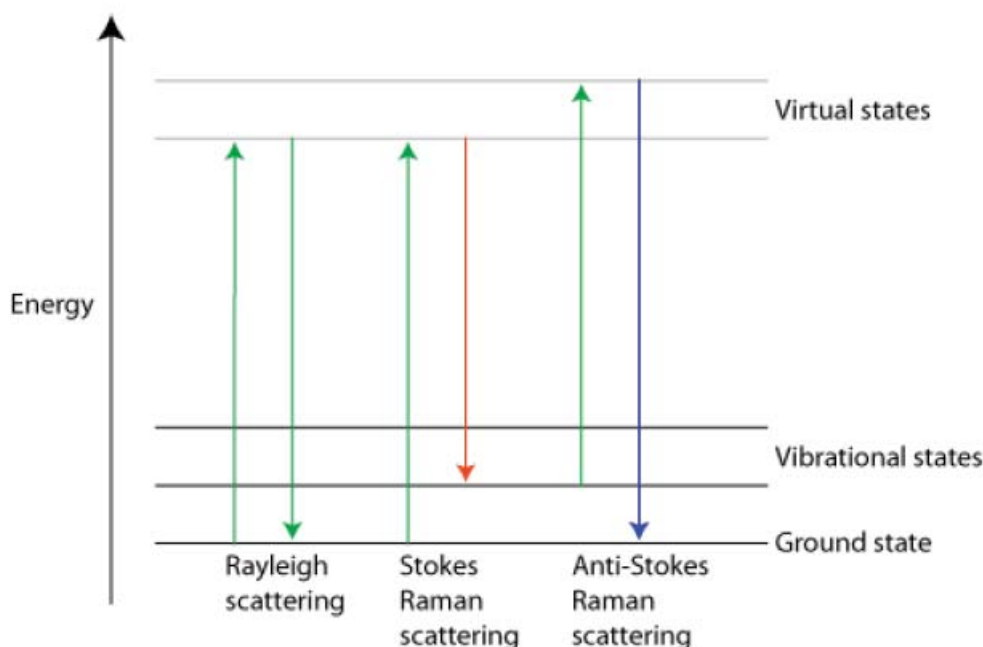


Figure 1: Energy diagram of the possible scattering processes [2]

Typically the intensity of the Rayleigh scattered light is 7-8 orders of magnitude greater than the Raman scattering, this means that from every $10^7 - 10^8$ scattering occasions only one photon will suffer Raman scattering (either Stokes or anti-Stokes). To detect Raman scattered light we must suppress the Rayleigh scattered light which is an important task in Raman spectroscopy as it is shown later.

We can see from Eq.4 describes that the energy of the Raman scattered photons depends on the energy of the frequency of the exciting light. To avoid this description the *Raman shift* $\Delta\nu$ (with the wavenumber dimension cm^{-1} unit) is introduced as the following:

$$\Delta\nu = \frac{1}{\lambda_{exciting}} - \frac{1}{\lambda_{scattered}} \quad (5)$$

Working in this scale allows us to analyze the Raman spectrum independently of the exciting energy as the Rayleigh peak is always at 0 cm^{-1} and the position of the Raman peaks are relative to the Rayleigh peak. Most of the literature uses positive Raman values for the Stokes range but the opposite can be also found see Fig. 2 The Raman scattering

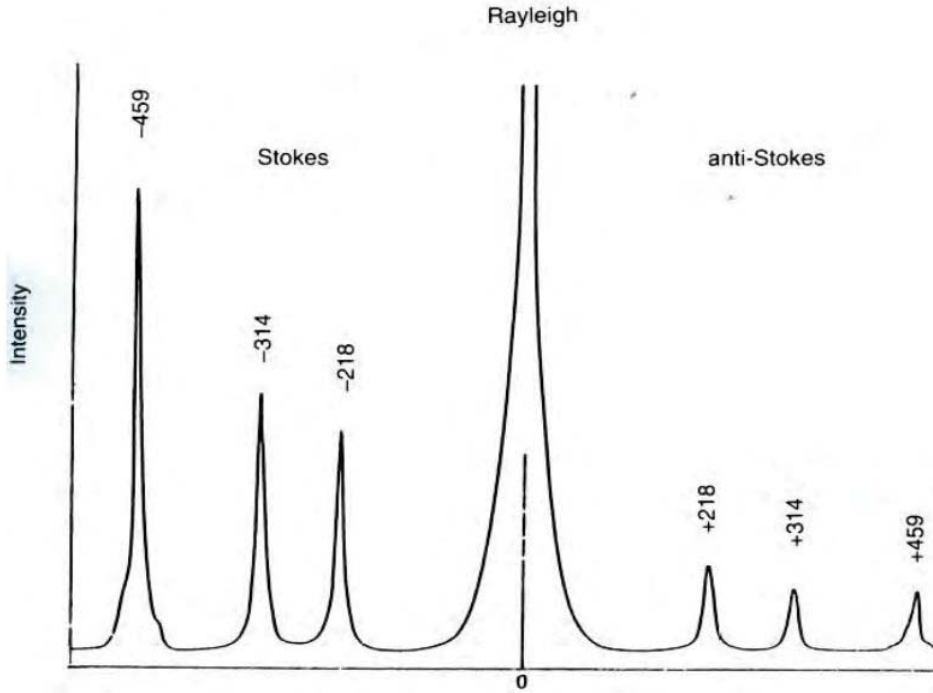


Figure 2: Raman spectrum of CCl_4 in Raman shift units. The position of Stokes- and anti-Stokes Raman peaks are symmetrical with respect to the Rayleigh peak at 0 cm^{-1} , but the intensity of Stokes Raman peaks are bigger than that of the anti-Stokes Raman peaks [3]

intensity is similar to the dipole radiation intensity. Without going into details [3] the Raman intensity I_R :

$$I_{Raman} = \sigma \omega^4 \alpha^2 E^2 \quad (6)$$

σ is a constant, ω is the angular frequency of the laser light, α is the degree of the polarisability and E is the electric field vector. Raman scattering has a strong ω^4 dependence of the laser angular frequency and it depends linearly in the exciting intensity.

2.2 General build-up of Raman spectrometers

There are two distinct types of Raman spectrometers depending on the method of separating the spectral components of the incoming light, namely the dispersive and Fourier transform (FT) spectrometers. In the Fourier transform spectrometers, the incoming light beam is guided into an interferometer, and the produced interferogram is analyzed. In dispersive Raman spectrometers, the light is analyzed with the help of optical gratings. Herein, we focus on the FT-Raman principle.

2.2.1 Excitation and light collection

In Raman spectroscopy monochromatic excitation is required, and because the Raman intensity is linear in the intensity of the excitation Eq. 6, applying laser as an excitation source is ideal as it has high spectral brightness. Eq. 6 also tells us that the Raman intensity depends on the fourth power of the excitation energy, which is the strongest dependence among the optical processes that can occur, hence it seems that applying a high energy laser source eg. UV laser would be the optimal choice. Applying UV lasers has two major obstacles: first it is not as practical as visible or infrared (IR) lasers because optical elements operating in the visible and IR regime are more better and cheaper than those of UV. The other important fact against using high energy lasers is that most materials have strong broadband luminescence response which is stronger than Raman peaks, making them undetectable. The luminescence intensity level increases with increasing the excitation energy in a non-linear manner. This is the main reason that for some materials (eg. carbon nano structures) IR laser source is used, because even visible lasers can cause the before mentioned effect.

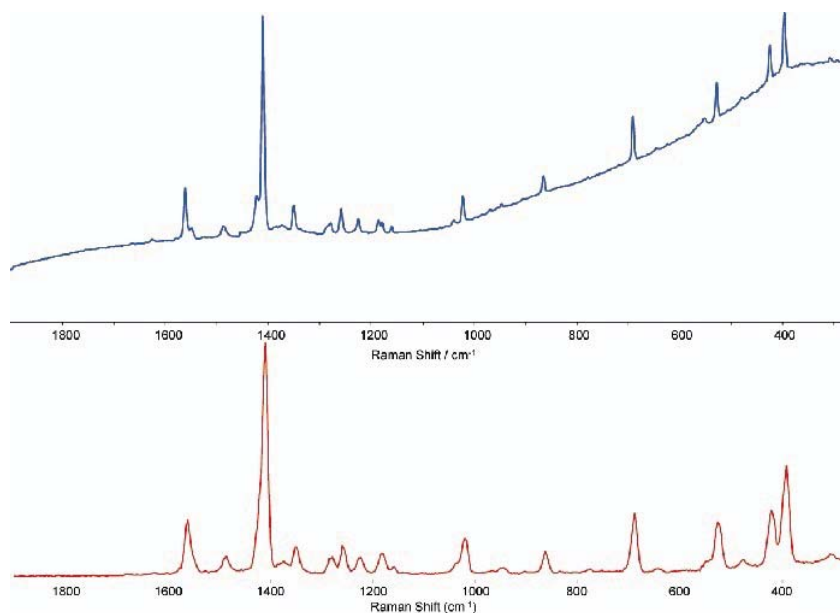


Figure 3: Raman peaks of 9-methylanthracene using 1064 nm laser (lower). Same spectrum using 796 nm laser, Raman peaks are located on a much intense broadband luminescent background for the latter [4]

The applied laser excitation can be classified as follows:

1. Gas lasers

The active media of the laser is gas usually He-Ne or Ar-Kr, they operate in several distinct lasing lines allowing to acquire spectrum for multiple different excitation lines.

2. Pumped tunable lasers

The active media is usually a dye (e.g. Rhodamin-6G) or crystal (e.g. Sapphire) they can be tuned to lase at a specific line in a broadband range (typically 100nm). These lasers are usually pumped by powerful solid state lasers. Such lasers are used in the so-called Raman mapping.

3. Solid state lasers

An example is the Nd:Yag laser, which operates at 1064. It is an efficient laser with a small footprint. The Nd:Yag crystal is pumped with solid state diodes at 810 nm. An intercavity frequency doubler also allows operation at 532 nm.

An important part of a Raman spectrometer is the collecting optics and especially the collecting objective. Because of the fact that the intensity distribution of Raman photons is isotropic it is crucial to collect the photons from a large solid angle. The efficient coupling of scattered (or Raman) photons into the spectrometer requires a delicate adjustment of the part of the sample which is illuminated by the laser: it should be in the focus of the objective and the collected light should be parallel to the optical axis of the spectrometer. The magnitude of the solid angle from which the photons are collected can be characterized by the *f-number* or $f/\#$ that reads:

$$f/\# = \frac{f}{d} \quad (7)$$

Where d is the diameter of the objective aperture and f is the focal length. Clearly, an objective with a small $f/\#$ is desired in Raman spectroscopy.

To choose the most suitable collecting objective we must consider the aberrations of an objective. Two aberrations are mentioned which are important from the view point of Raman spectroscopy:

1. Spherical aberration

Spherical aberration is the phenomenon when the light rays parallel to the optical axis but with different distance of it has different focal length, that is an aperture dependent focal length.

2. Chromatic aberration

Chromatic aberration occurs due to the fact that the refractive index of the objective depends on the wavelength of the incident light, and as the focal length depends on the refractive index, incident light with a broadband spectrum will have several focal length, that is a wavelength dependent focal length

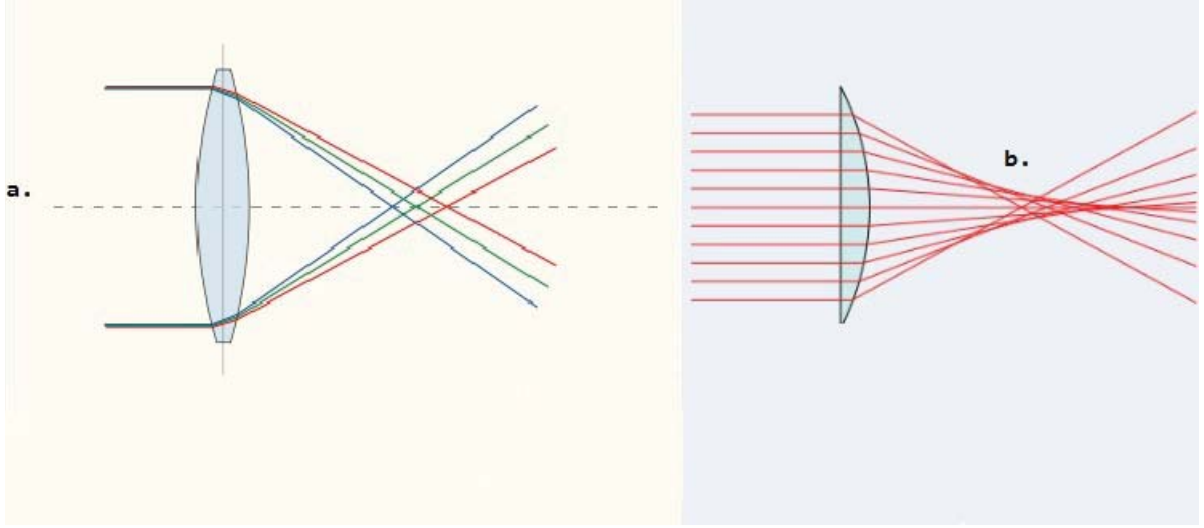


Figure 4: Exaggerated scheme of chromatic aberration in a., Fig b. demonstrates the spherical aberration.[5] [6]

These aberrations are demonstrated in Fig. 4. In Raman spectrometers the light beam is guided through *pin holes* and apertures, and because the Raman spectrum is a broadband spectrum usually up to (5000 cm^{-1} bandwidth), it is important to use an achromatic and aspheric lens to prevent intensity losses. The use of reflective rather than refractive elements wherever possible, leads to an improvement in tackling chromatic aberration.

2.2.2 Fourier transform spectrometers

The heart of every optical spectrometer is the way they separate the spectral components of the incoming light. In FT-spectroscopy, the separation is achieved due interference by introducing an interferometer. Interference of light occurs when monochromatic, coherent light are superimposed in a phase coherent manner. Suppose two electromagnetic waves (having the previously mentioned attributes) with the same intensity I_0 are superposed, where:

$$\begin{aligned} \underline{E}_1 &= \underline{E}_0 e^{i(kr - \omega t)} \\ \underline{E}_2 &= \underline{E}_0 e^{i(kr - \omega t + \delta)} \end{aligned} \quad (8)$$

The detected intensity is the square of the absolute value of the sum of the two wave components, which gives:

$$I = |\underline{E}_1 + \underline{E}_2|^2 = 2I_0(1 + \cos \delta) \quad (9)$$

In an interferometer, the phase difference is achieved by letting the two wave components travel different optical paths, due to the *Optical Path Difference* or *OPD* a phase shift will appear in one wave, with respect to the other $\delta = OPD(r) \frac{2\pi}{\lambda}$ thus if the OPD is $n\lambda$ then we get constructive interference, while if OPD is $(2n+1)\frac{\lambda}{2}$, then we get destructive interference where n is an integer: see Fig. 5.

We discussed the case of two monochromatic waves above, now we consider the case of broadband source, that have a wavenumber dependent energy density (spectrum) $E(k)$,

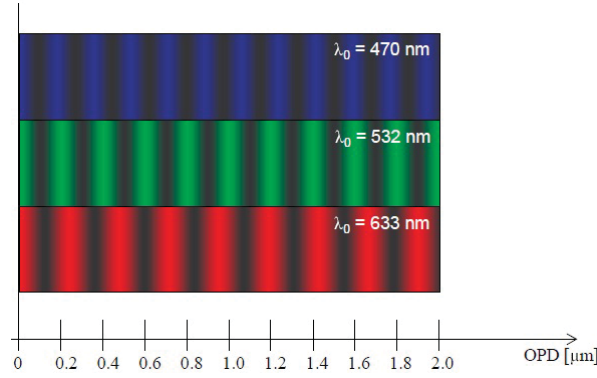


Figure 5: Interference pattern of electromagnetic waves of different frequency in terms of the Optical Path Difference, radiation with smaller wavelength has an interference pattern with higher frequency [7]

now let us consider the intensity distribution of the interference pattern of the spectral components between k and $k + dk$. Applying Eq. 9 we obtain $dI(k, x) = 2E(k)(1 + \cos kx)dk$, this is called *interference record*, by defining $E(x) = E(-x)$ we can construct the following $F(x)$ function:

$$F(x) = \int_{-\infty}^{\infty} 2E(k)(1 + \cos kx)dk \quad (10)$$

From the interference record we can retrieve the intensity distribution: the *interferogram*

$$I(x) = F(x) - \frac{1}{2}F(0) = \int_{-\infty}^{\infty} 2E(k) \cos(kx)dk \quad (11)$$

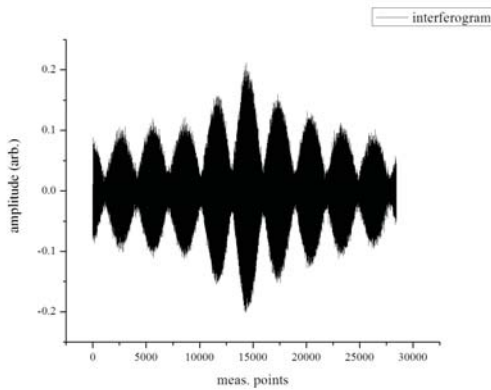


Figure 6: A typical interferogram of a broad band source and its spectrum in Fig 5. [8]

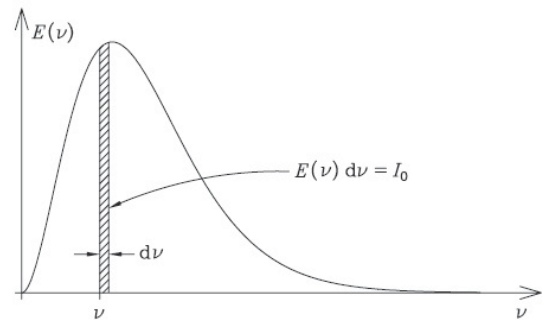


Figure 7

The interferogram is the Fourier transform of the spectrum of the source, thus applying

inverse Fourier transformation we can obtain the spectrum:

$$\begin{aligned} I(x) &= \int_{-\infty}^{\infty} 2E(k)e^{ikx} dk \\ E(k) &= \frac{1}{2} \int_{-\infty}^{\infty} I(x)e^{-ikx} dx \end{aligned} \quad (12)$$

The major role of an FT interferometer is to acquire the interferogram, as every information of the source is contained in it. Generally in optical FT-spectroscopy, the interferogram is produced by an interferometer. The most commonly used type is the *Michelson interferometer* Fig. 8.

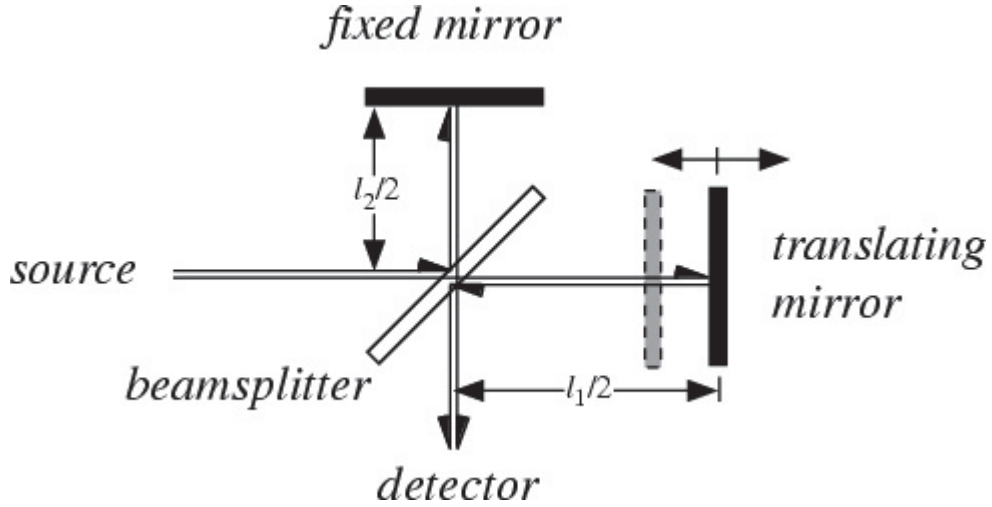


Figure 8: The schematic of a Michelson interferometer, incoming light is separated by a beam splitter, one beam travels towards a fix mirror the other towards a moving mirror which introduces a relative phase shift, the two beams are united and detected, interferogram is recorded [9]

The interferometer itself is relatively simple: light enters from the source, and is divided by a beam splitter which ideally transmits half- and reflects half of the intensity. The first beam is sent towards a fixed mirror which reflects it backwards the beamsplitter. The second beam is sent towards a moving mirror and again reflected towards the beamsplitter, then the two beams are unified and sent towards the detector. Due to the difference in the path of the two beams, the intensity on the detector will be modulated according to Eq. 12. The critical part in a Michelson interferometer is the moving mirror, as it controls the optical path difference, which produce the δ phase shift. The moving mirror moves with a fixed velocity between the two endpoints of the range of motion of the mirror, the produced interferogram will be sinusoidal in time as $\delta = \frac{2\pi}{\lambda} OPD(t)$ where $OPD(t) = vt$ where v is the mirror velocity, thus $\cos \delta = \cos(\frac{2\pi}{\lambda} vt)$ Fig 9.

2.2.3 Sampling and the He-Ne laser

A great advantage of the FT-Raman rinciple over dispersive spectrometers, is the accuracy of the wavelength measurement. A critical part of the apparatus is the sampling mechanism which relies on the built-in He-Ne laser source.

The properties of the He-Ne:

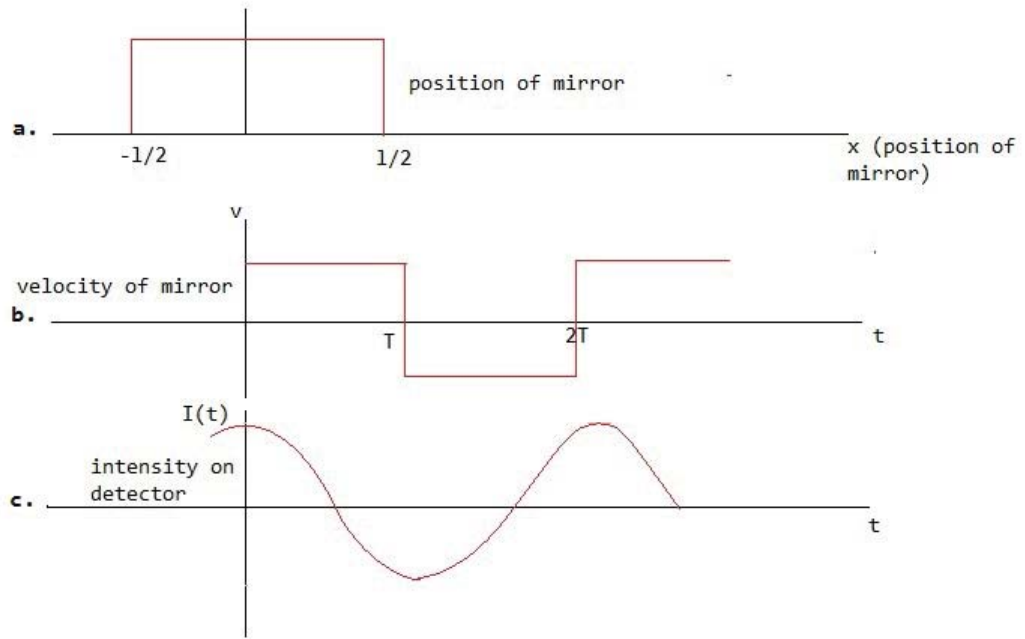


Figure 9: Fig. a. shows the position of the mirror which moves between $-\frac{l}{2}$ and $\frac{l}{2}$. Fig. b. shows the velocity of the moving mirror which moves uniformly back and forth. Fig. c. shows the detected interferogram produced by the uniformly moving mirror

1. $\lambda = 632.832nm$
2. $f = 473.6THz$
3. $k = 15797 cm^{-1}$
4. $E = 1.96eV$

The spectrometer uses He-Ne laser as a reference. Reference means two important things in the case of spectrometer:

1. The wavelength of 632.832 nm is considered the reference signal with a frequency of 1 Hz, every other measured frequency is calibrated with respect to this reference.
2. The electronic unit takes data twice during one period of the interference pattern of the He-Ne laser, each times the interferogram is 0, which occurs when $OPD = \frac{\lambda}{2} = 316.41nm$, which is a technically robust and a relatively simple sampling method.

Fig 10 and Fig. 9 is a visual representation of the sampling mechanism of a FT-spectrometer. The calibration procedure against the He-Ne laser is as follows. The He-Ne ($632.832nm$ $15797 cm^{-1}$) interferogram is sampled when it crosses the zero and its frequency serves as a standard and can be regarded as 1 Hz. Now suppose we want to detect a monochromatic radiation of unknown frequency (but longer wavelength than $632.832 nm$): the produced sinusoidal interferogram of the unknown radiation will be proportional to that of the He-Ne interferogram, where the proportion factor is the quotient of the He-Ne wavelength to the

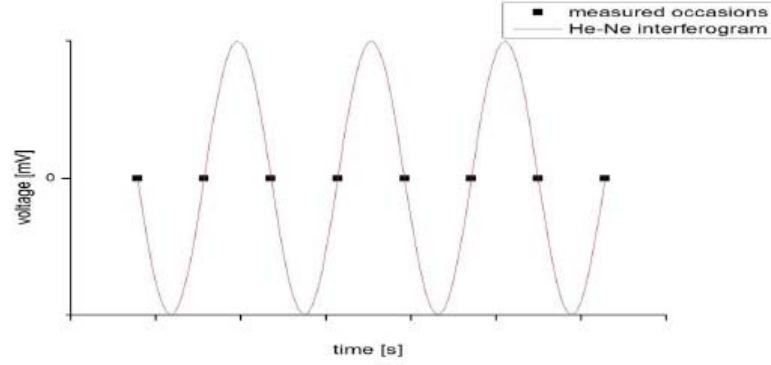


Figure 10: Interferogram of the reference He-Ne laser is detected by an AC resulting in a cosine function, measurement points are taken whenever the intensity of the interferogram is 0

unknown wavelength $\frac{\lambda_{He-Ne}}{\lambda_{unknown}}$ which is less than one, by acquiring the interferogram of the unknown radiation, we can calculate this proportion factor, from which the absolute wavelength $\lambda_{unknown}$ can be obtained. For example if we irradiate the spectrometer with the laser line of Nd-YAG i.e. $1064nm$, $9398.cm^{-1}$, the proportion factor will be 0.59 thus the spectrometer will acquire an interferogram that has a frequency of $0.59 Hz$. Naturally the detection principle is the inverse of the previous i.e. the spectrometer will detect an sinusoidal interferogram that have a frequency of $0.59Hz$, and the unknown wavelength will be calculated by dividing $\frac{632.832}{0.59} nm = 1064 nm$.

2.2.4 Effect of sampling parameters on intensity

Resolution

Measured signal is recorded for finite time, this can be imagined as infinite signal in time, that is multiplied by a *rect* function, which is a rectangular window that will allow only a finite "slice" of the signal, this is called *truncation*. Obviously the spectrum of a truncated signal will differ from an infinite one.

The effect of truncation will manifest in the resolution of the spectrum, which by definition is the *Full Width at Half Maximum* or *FWHM* of the peak in the spectrum. Now let us denote the truncated signal by $h_T(t)$, and the original signal $h(t)$, where $h_T(t) = h(t)rect(T)$, where $rect(T)$ is a T wide rectangular window centered at the origin. The Fourier transform of the truncated signal i.e. the two multiplied function will be the convolution of the Fourier transform of the two functions according the law of convolution: $F(h(t)g(t))(\omega) = H(\omega) * G(\omega)$, now $F(rect(t))(\omega) = 2T\frac{\sin \omega T}{\omega T}$, which is also known as the *Sinc* function.

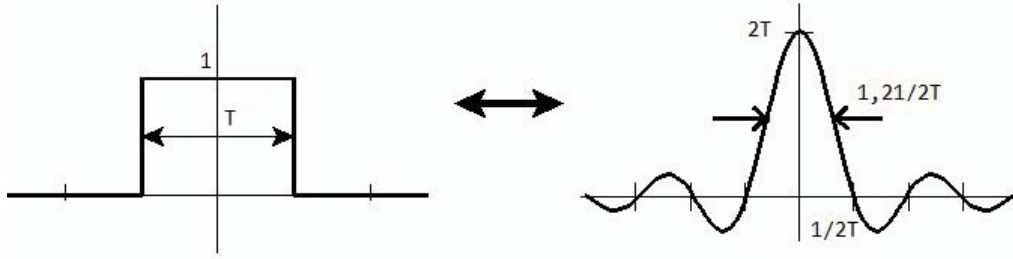


Figure 11: The Fourier transform of a T wide rectangular function is a Sinc function, where the FWHM is $\frac{1,2T}{2T}$ is defined as the resolution [10]

In case of a discrete spectrum, eg. two Dirac deltas centered at ω and $-\omega$, we will have two sinc functions instead, centered at the same position.

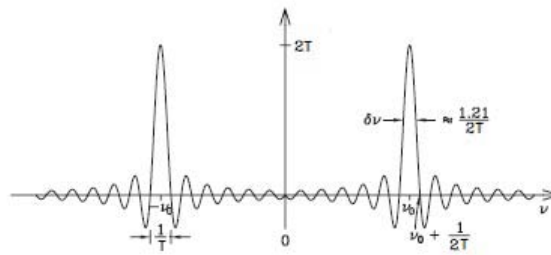


Figure 12: the spectrum of a truncated cosine function, instead of two delta functions there are two sinc function present [8]

We note that the FWHM of the signal is directly proportion to the inverse of the measurement time. The range of motion of the mirror is directly proportional to the measurement time, hence the spectral resolution is determined and bounded by the range of motion of the mirror. $FWHM \sim \frac{1}{T}$

In case of FT-spectroscopy, the interferogram is recorded while the mirror is moving. There are four major acquisition modes which specifies the movement of mirror:

1. *Single-sided*: the mirror starts at the beginning of the range of motion rather than in the middle, thus the mirror moves from 0 to $2L$ rather than from $-L$ to L , and we assume that the spectrum is even $E(t) = E(-t)$, thus we double the width of the *rect* function. Data is acquired during the forward movement of the mirror . In this mode the spectral resolution is high.
2. *Double-sided*: Data is acquired during the forward movement, mirror moves from $-L$ to L . Signal to noise ration is better-, spectral resolution is lower than the *single sided*
3. *Forward-backward*: Spectrum is acquired during the forward, and backward movement of the mirror, the acquired spectra are coadded, signal to noise ratio is better but acquisition time is longer.

4. *fast return*: data is collected during the forward movement of the mirror, backward movement is done rapidly, without data acquisition.

Now, we consider an example for a typical spectrometer setup with the Nd-YAG laser working at 1064 nm. The typical instrument settings are:

1. Mirror velocity: 5kHz
2. Resolution: $\Delta k = 4 \text{ cm}^{-1}$
3. Acquisition mode : Forward-backward

The sampling frequency is 5kHz, which means that the electronic unit will take one measurement point every 0.2 ms, as the He-Ne interferogram guides the sampling rate ($T_{He-Ne} = 0.4 \text{ ms}$), acquiring N measurement points will take $T_{meas} = N * T_{He-Ne}$ as there are two measurement points in one He-Ne period. The resolution according to Fig. 11 is:

$$\Delta f = \frac{1.21}{2T_{meas}} \quad (13)$$

Here $\Delta f = \Delta k c = 0.012 \text{ THz}$ where c is the speed of light. As the Nd-YAG frequency is 120 THz the relative resolution is $\Delta f_{rel} = \frac{\Delta f}{f} = 4.27 \cdot 10^{-5}$. As mentioned before the electronic unit saves the as $f_{He-Ne} = 1 \text{ Hz}$ thus the relative resolution Δf_{rel} and $T_{He-Ne} = 1$ is substituted in Eq. 13 which means that $T_{meas} = 2N$, thus for a $\Delta k = 4 \text{ cm}^{-1}$ resolution, the number of measurement point is:

$$N = \frac{1.21}{4\Delta f_{rel}} = 7184 \text{ measurement points} \quad (14)$$

Acquiring one scan will take $T_{meas} = 7184 * 0.2 \text{ ms} = 1.4 \text{ sec}$. In general equation of the resolution Δk of FT-spectrometers around k absolute wavenumber is:

$$\frac{\Delta k}{k} = \frac{1.21}{4N} \quad (15)$$

2.2.5 Advantages of the FT technique

The FT technique provides several advantages over dispersive spectrometers [11]

1. Connes advantage:

Due to the complex mechanical parts which control prisms or gratings in dispersive spectrometers, there is an inherent inaccuracy problem in dispersive spectrometers as the peak position will slightly change from scan to scan. Due to this uncertainty of peak position, repetitive calibration must take place. On the other hand the built-in He-Ne laser, acts as a reference which means that the wavelength calibration is done automatically in every spectrum, since sampling occurs at the zero crossing of the He-Ne interferogram (caused by the translation of the mirror). Thus the wavelength accuracy only depends on the wavelength stability of the He-Ne laser, which is high due to it being a gas laser. cm^{-1} .

2. Jacquinot advantage:

The spectral resolution in dispersive spectrometers depends on the size of the entrance slit. As an example, a typical dispersive spectrometer yields 1 cm⁻¹ resolution if the slit is 100 micron large. Introducing a narrow slit causes a tremendous loss of photon number i.e. light intensity on the detector. On the other hand resolution in FT-spectroscopy is determined solely by the range of motion of the translating mirror, allowing to operate with big apertures, this means that a much higher SNR can be achieved by FT-spectrometers. This advantage is also known as the *throughput* advantage.

3. Fellgett or multiplex advantage:

Dispersive spectrometers acquire the spectrum by rotating the grating, recording one spectral component after the other. In case of FT-spectrometers every spectral component is present in the interferogram simultaneously. The measurement time of one spectrum is bounded by the velocity of the moving mirror, thus one spectrum can be recorded in a matter of seconds. This means that during the time it takes a dispersive spectrometer to acquire one spectrum, FT spectrometers can acquire several and average them, resulting in a significantly better SNR.

3 Experimental methods

3.1 Reference sample

The signal

The main aim of this thesis is to summarize the development of three spectrometer configuration. In order to qualify the performance and the signal to noise ratio of the spectrometers and to monitor the development stages we used sulphur as a reference sample due to the fact that sulphur has very strong and narrow Raman peaks between 0cm^{-1} and 3000cm^{-1} .

Sulphur has its strongest peak at 218 cm^{-1} , when calculating the signal to noise ratio the peak at 218 cm^{-1} was taken as signal.

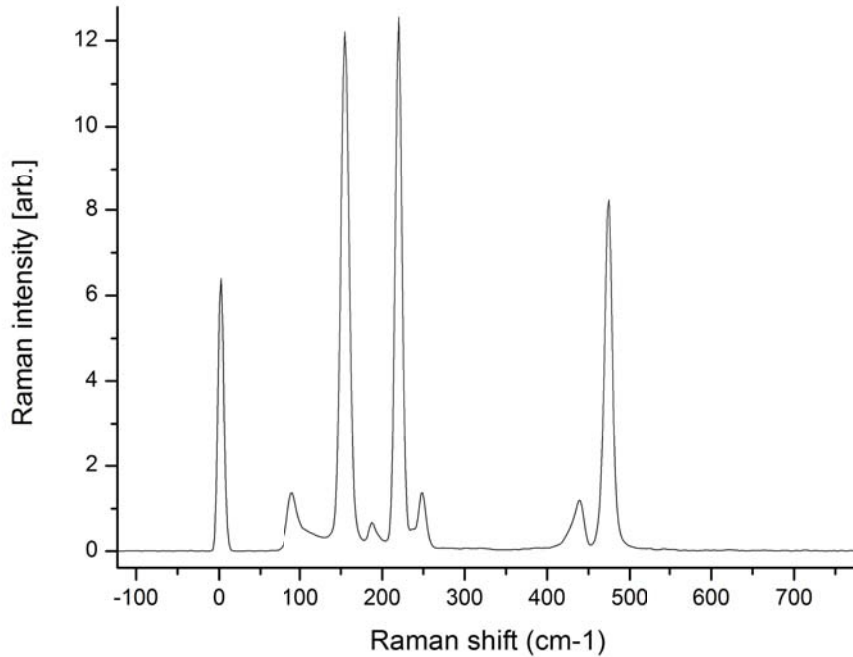


Figure 13: The Raman spectrum of sulphur. The most intense peak at 218 cm^{-1} . Signal to noise ratio in this thesis was calculated taking the peak at 218 cm^{-1}

The noise

An important factor in the quality of a spectrum is the *Signal to noise ratio* or SNR. Every measurement is burdened by noise, which is every undesired signal in the spectrum. The relationship between the noise level P_{noise} and the signal level P_{signal} is the SNR, that is defined as $SNR = \frac{P_{signal}}{P_{noise}}$.

One desires to optimize SNR, as it reduces the measurement time for a sample, or allows spectroscopic access to samples with lower signals, too. We can reduce the noise by averaging spectra: according to the *Central Limit Theorem* if we average N spectra the noise will decrease by a factor of \sqrt{N} thus the dependence of the signal to noise ration on the measurement time T_{meas} will be $SNR \sim \sqrt{T}$ (see Appendix). The measurement noise was calculated from the spectral region from $1000cm^{-1}$ to $2500cm^{-1}$, where sulphur has no Raman modes.

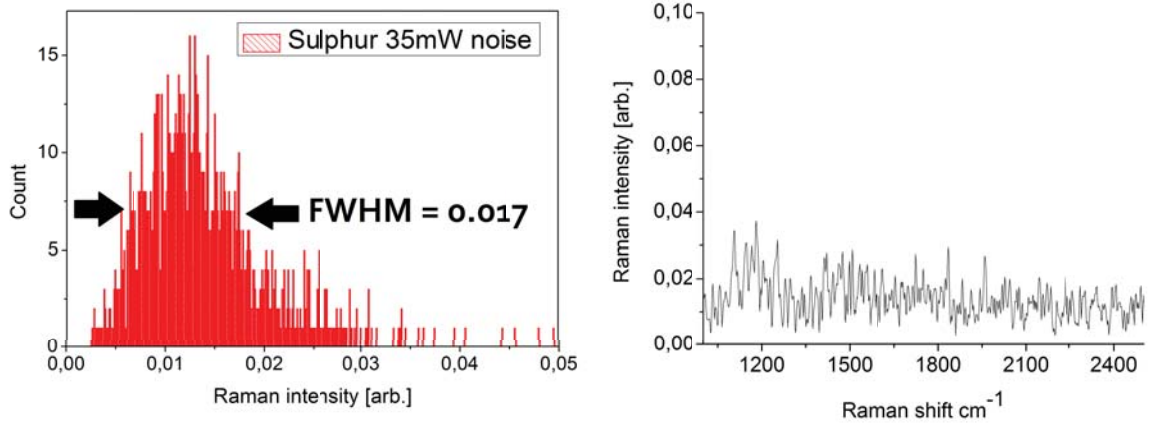


Figure 14: At the right is the part of the sulphur Raman spectrum which is considered for the noise calculation from $1000cm^{-1}$ to $2500cm^{-1}$. Left figure is the histogram of the noise, that is considered as the FWHM of the histogram.

The statistical standard deviation, σ of the noise is identical of the half width at half maximum of the noise histogram as show in Fig 14.

3.2 The modern interference filters

It was mentioned in the previous section that Raman scattering process is a weak process and the intensity of the Rayleigh photons is seven-eight orders of magnitude greater than the intensity of Raman photons. This becomes a problem when we want to detect the Raman photons: because of the weak intensity of the Raman photons we have to use very sensitive detectors, that have saturation intensity way lower than the intensity of Rayleigh photons, that is if we do not suppress the Rayleigh photons, we will not be able to detect anything. In the past few decades optical filtering was done by the so-called subtractive monochromator that is light was guided to an optical grating, and the Rayleigh (excitation) peak was removed physically from the resolved spectrum, after which the rest of the spectrum was reunited with another grating, thus the light exiting the filter would miss the spectral component at the excitation line. This realization of optical filter works as a band pass filter but it had several disadvantages: applying gratings is expensive and has a need of space, also the cut-off edge around the Rayleigh peak was not as steep as it should have been and depends on the quality (resolution) of the grating and the spatial extensions of the filter, but the main problem was the transmission of the light intensity, as it was relatively poor due to the need for several optical elements: 2 gratings and a few (at least 4) mirrors.

The problem was solved by the development of the thin layer technology when the thin layer interference filters became commercially available, making a considerable progress in the intensity transmission of the spectrometers. Interference filter is a series of thin dielectric coatings on a transparent bulk material, the coated layers have different refractive index, a layer with high refractive index is followed by a low refractive index making a high refractive index gradient. Light reflected from the surface of a specific layer interferes with the light reflected from every other surface, by manipulating the thickness of the coating the interference intensity can be manipulated eg. it can be achieved for a specific wavelength to have a constructive maximal interference resulting in the total reflection of the light (eg. by choosing the thickness of the layers to be $\frac{\lambda}{4}$), while the transmission of other wavelength suffer negligible losses. The quality of the filter eg. cut-off edge steepness depends on the number of layers deposited, and the quality of the refractive index gradient, with contemporary surface technology the properties of interference filters can be enhanced considerably with respect to other types filters.

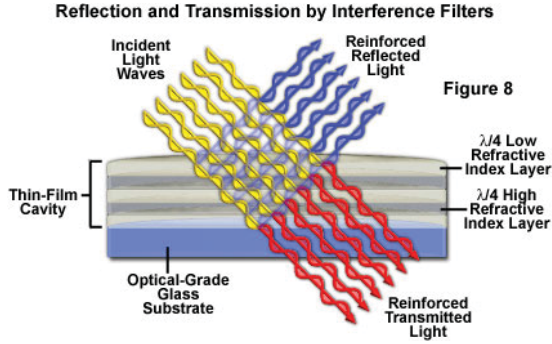


Figure 15: A schematic of the structure and functioning of interference filter. With $\frac{\lambda}{4}$ thick coatings, sub wavelength refraction index gradient is achieved. figure by *Olympus inc.* [12]

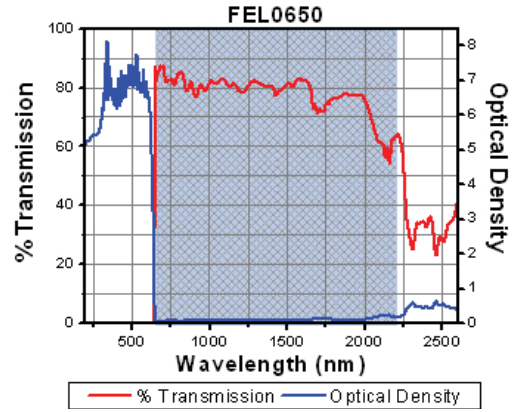


Figure 16: A typical transmission of a long-pass interference filter produced by *Thorlabs* in terms of transmission and optical density (OD). Figure by *Thorlabs*[13]

3.3 The detectors used in FT-Raman spectroscopy

3.3.1 NIR photodiode

The detector used in IFS66V IR spectrometers is a *Bruker D418-T* Germanium (Ge) solid state detector cooled by liquid nitrogen [14] in order to reduce its thermal noise. A solid state detector is an closed biased p-i-n junction (photodiode) see Fig. 17. Photons absorbed in the intrinsic layer will excite an electron-hole pair that will be converted to detectable electrical current due to the applied voltage. Three parameters characterize the detector performance: the electronic cut-off frequency which determines the the bandwidth for amplitude modulated signals, the *Noise Equivalent Power* or NEP which determines the smallest detectable signal and the saturation level which determines the biggest detectable signal.

The cut-off frequency

A photodiode detector can be considered as a low pass filter, modeled in Fig. 18 The amplitude of the output signal is determined by the *Gain* factor (G) see Eq.16

$$G = \frac{U_{out}}{U_{in}}$$

$$where \ U_{out} = U_{in} \frac{Z}{R + Z} = U_{in} \frac{1/i\omega C}{R + 1/i\omega C} = U_{in} \frac{1}{1 + iR\omega C} \quad (16)$$

$$G = \frac{1}{\sqrt{1 + (R\omega C)^2}}$$

Here Z is the impedance of the capacitor, R is the resistance, C is the capacitance, ω is the angular frequency of the signal.

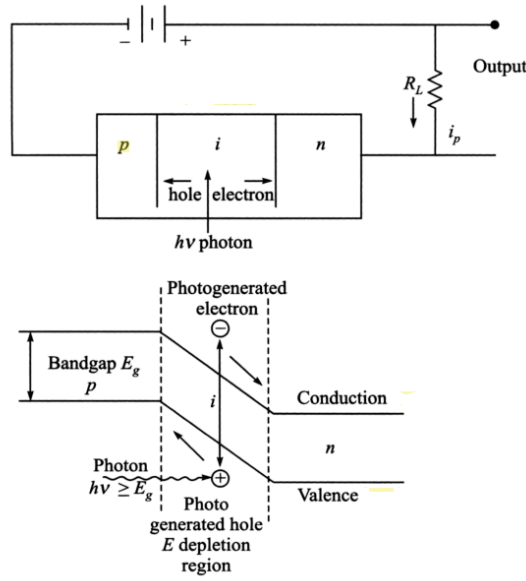


Figure 17: Schematic buildup of a solid state detector. The schematic energy band structure is shown along the length of the device [15]

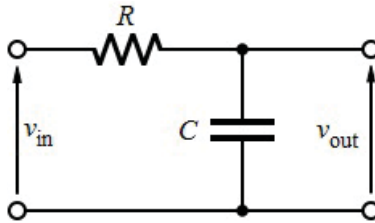


Figure 18: the photodetector can be considered as a low pass filter

The gain factor decreases as the input signal frequency increases. The cut-off frequency of the detector is defined as the frequency where $G = \frac{1}{\sqrt{2}}$ the input amplitude, in which case $\omega_{co} = \frac{1}{RC}$, this means any signal, amplitude modulated with a higher frequency than ω_{co} will be attenuated considerably. The signal produced by the interferometer is time dependent, because the detected light intensity is periodically amplitude modulated due to the movement of the interferometer mirror.

In order to characterize the detector the Raman spectrum of a sulphur was taken at different sampling rates. It is seen from Fig. 19 that the cut-off frequency is 5kHz.

Detector quality and Noise

The Ge photodiode noise was measured both in time and frequency domain, also with and without incident power. The noise is detector noise limited for low optical power i.e. the noise dose not depend on the power of the detected radiation. The characteristic noise levels are shown in Table 20

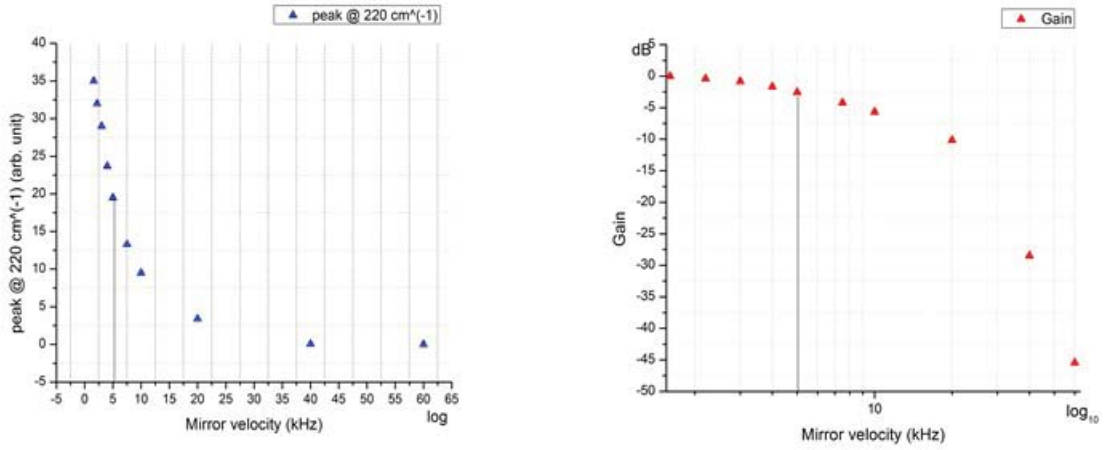


Figure 19: Through-put function of the applied Ge photodiode in IFS66v, both in linear and log scale. The reference input signal was considered the signal at 1kHz mirror velocity. The cut off frequency is 5 kHz

Sample: Sulphur in plexi holder

Source: Nd-YAG 1064 nm laser

parameters: 5 kHz sampling freq. and 4cm^{-1} resolution

		Power on sample (mW)	Noise level
Spectrum	measured in OPUS	0	0,006 arb. unit
		35	0,015 arb. unit
Time domain	measured with Oscilloscope	0	11mV 6,5 mV RMS
		35	not possible

Figure 20: Noise values are given in units of the OPUS measurement program. Noise level in the time domain was not measurable in oscilloscope as the image is a spread interferogram

An important quantity expressing the quality of photodetectors is the *Noise Equivalent Power* or NEP. A photodetector will produce noise even when there is no incident power on it, the NEP is a good quantification of this noise level, as by definition NEP is the incident power level of 1Hz bandwidth signal, that will yield an output power equivalent with that of the noise, or in other words: the incident power level that will produce a $SNR = 1$, thus it is the smallest 1Hz wide signal which is detectable. The total noise is expressed in the following equation: $Noise = NEP \times \sqrt{Bandwidth}$.

Detector used in Bruker IFS66V Raman module is a *D418-T* part No. liquid Nitrogen cooled Ge photodetector, that has $NEP < 10^{-15} \text{W Hz}^{-1/2}$. The NEP of the detector can be checked if the attenuation of the optical filter is known: using the same parameters in table Table Fig. 20 we measured 10mW power in front of the optical filter, this

corresponds to the Rayleigh peak. In our case the optical attenuation is OD6 (*Optical Density*) that is 10^{-6} , other optical losses is estimated to be OD1 due to the beamsplitter and other optical elements so the Rayleigh intensity on the detector is :

$$\text{Signal} = 10\text{mW} \times \text{OD6} \times \text{OD1} = 10^{-9}\text{W}$$

$$\text{Noise} = \text{NEP} * \sqrt{\text{Bandwidth}} = 10^{-15} \times \sqrt{5000} = 7 \times 10^{-14}$$

$$\text{SNR} = 1400$$

Also we know the spectral noise level from table Table Fig. 20 and the Rayleigh peak intensity from the spectrum:

$$\text{Noise} = 0,006,$$

$$\text{Signal} = 3$$

$$\text{SNR} = 500$$

The difference between the measured and estimated SNR is a factor of 2,8 which means that the which means that the NEP we measure is consistent the the value given by the manufacturer.

3.3.2 The photomultiplier tube

We use a photomultiplier tube in our development of a visible FT-Raman spectrometer. In order to understand the magnitude of the detected signal and the nature of the noise the detection principle must be understood. A PMT detector is based on the phenomenon of photo emission of metals. The incident photon is absorbed in a layer capable of photo emission (usually Multialkali layer), this is called the photocathode. The cathode is followed by a series (typically 9 or 10) of Multialkali electrodes (dynodes) where voltage is applied between every dynode pair, at the end there is the anode. An emitted photo-electron is accelerated due to the voltage applied between the dynodes, when the electron hits a dynode secondary electrons are emitted, and further accelerated towards the next dynode, the process continues till the amplified current reaches the anode.

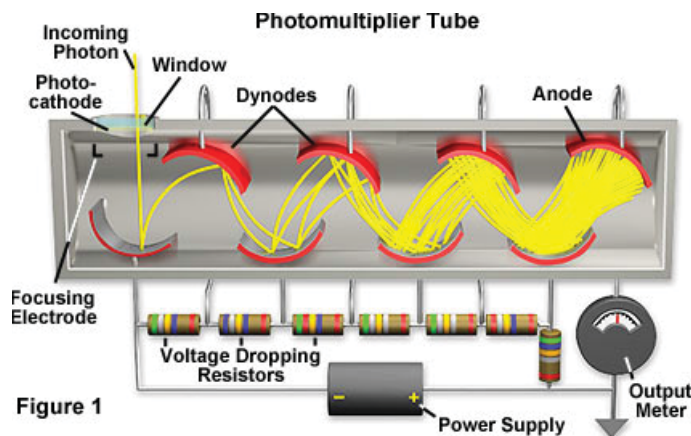


Figure 21: Visalisation of the mechanism of a PMT. The emitted photo-electron is accelerated, emitting secondary electrons on the dynodes, in the end a measurable current is present on the anode [16]

The ability of the photocathode to emit photoelectrons is given by the quantum efficiency

(QE). QE is the probability of a photon to induce a photoelectron, that usually varies between 10% – 20%, depending on the wavelength of the radiation Fig. 23. The overall sensitivity of the cathode is described by the cathode radiant sensitivity in mA/W units, which gives the generated cathode current due to the incident radiation power Fig. 23.

The voltage applied between the dynodes can be adjusted linearly with applying control voltage. Depending on the ability of the secondary electron emission of the dynodes and the applied voltage, the sensitivity of a PMT is given by the gain factor g which shows that with given cathode current I_c induced by the absorbed photons the anode current will be $I_a = gI_c$ Fig 22. The work function of a typical metal is about 2 eV. A visible photon has sufficient energy to generate a photoelectron. Then the electron is accelerated typically to 100 eV until it reaches the next dynode, and it thus generates about 5-10 secondary electrons. This gives rise to a typical gain of up to $10^7 - 10^8$.

In order to make the output signal of the PMT displayable, it was connected to a *HAMAMATSU C7319 Amplifier unit* I/V converter [17] (that serves also as signal amplifier) with 15V operation voltage, that can be configured to operate with two optional bandwidth, and three different gain factors listed in the following table:

operational bandwidth (BW)	gain factor (g)
20 kHz	10^5
200 kHz	10^6
	10^7

The output voltage of the I/V converter is divided to two, one is monitored by an oscilloscope, the other is connected to the detector input slot of the spectrometer.

The main noise source when using a PMT is the so-called shot noise see Section 4.3.1. Shot noise is proportional to the square root of the incident radiation power, i.e. it can only be improved by increasing the incident photon flux or by improving the QE of the photo-cathode, and it is independent of the PMT gain or the gain of the I/V converter.

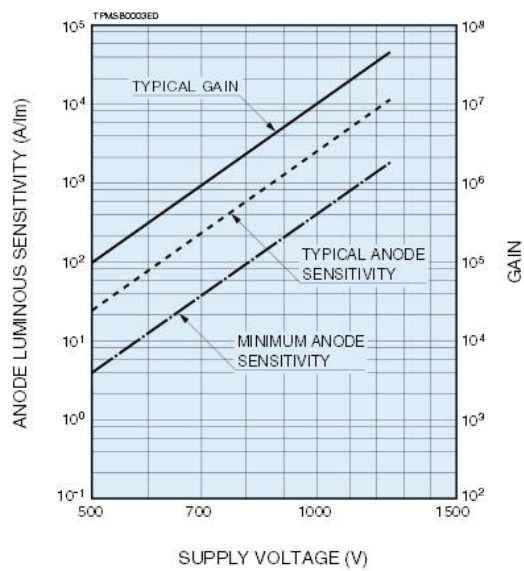


Figure 22: The gain of the *Hamamatsu R955* PMT as function of the applied voltage (dashed curve) [18]

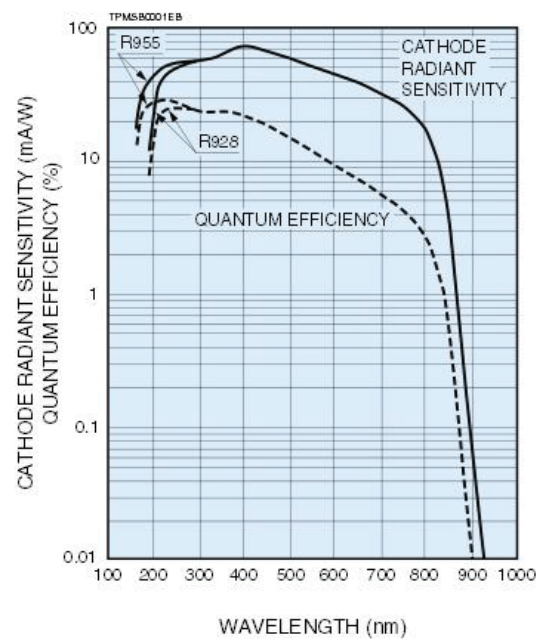


Figure 23: The QE and cathode radiant sensitivity of *Hamamatsu R955* PMT as function of radiation wavelength [18]

4 Results and discussion

4.1 Optical upgrade of a commercial FT-Raman spectrometer

4.1.1 Optical path and filters

Source and guiding optics

It is important to have an aspheric collecting objective, as we use objective with small $\frac{f}{\#}$. The simplest aspheric objective is an aspheric singlet (i.e. one lens). The sample is placed in the focus point, and the scattered Raman light is collected and collimated. The Bruker Raman spectrometer has such a large diameter aspheric singlet as a Raman light collection objective. It suffers from chromatic aberration, however, it is not very significant for a narrower Raman range. We have tested a chromatic aberration free collection objective (the *Navitar D0 5095* with $f/\# = 0.95$) but it did not improve substantially Raman signal. We note that it is partly due to this objective being optimized for the VIS range. The ultimate solution could be a lens system objective, which is corrected for both chromatic and spherical aberration and optimized for the NIR range. Such objectives are available commercially (for night vision) but this are expensive (over 4000 Euro).

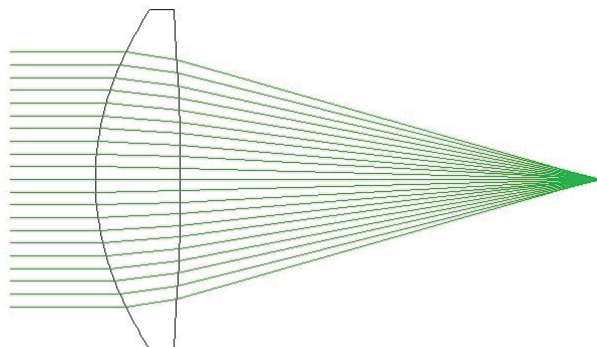


Figure 24: A simple aspheric singlet (Plano-convex) used in IFS66V spectrometer. The sample situated in the focus of the objective

Optical filter

Originally, the spectrometer was not operational, and several smaller parts had to be repaired first: the power supply of the Nd:Yag laser was not functioning, all interconnects were dismantled, the spectrometer was fully misaligned optically, and the cryostat of the Ge detector was soft.

After studying the performance of the detector and the guiding/collecting optics, a benchmark measurement was made with the following parameters and measured SNR Fig. 25. After recovering the spectrometer into working condition the measured SNR was 170. The data sheet supplied by the manufacturer *Bruker Inc.* stated that the optimal SNR is

300, the spectrometer operated worse with a factor of two than the manufacturer benchmark (this benchmark).

Sample	Sulphur in plexi holder
excitation	1064 nm
power on sample	85mW
sampling frequency (mirror velocity)	5kHz
resolution	4cm ⁻¹
Signal (peak @ 218 cm ⁻¹)	2,55 arb. unit
Noise (estimated)	0,015 arb. unit
SNR	170

Figure 25: Benchmark parameters and measured SNR after recovering Bruker IFS66V spectrometer

The original Rayleigh filter has a huge size size and poor throughput; the transmission of the original filter in IFS66V is about 15%.

The first step of the optical upgrade of Raman spectrometer took place in October 2011. The spectrometer's original low-throughput Rayleigh filter was replaced by a *Semrock Razor edge* 1064 nm Long Pass (LP) Filter. The throughput characteristic of the filter is shown in Fig. 26; It has nearly 100% (OD0) transmission in the pass band and OD6 suppression for the stop band with a transition range of only 93 cm⁻¹, between 10-90 % transmission.

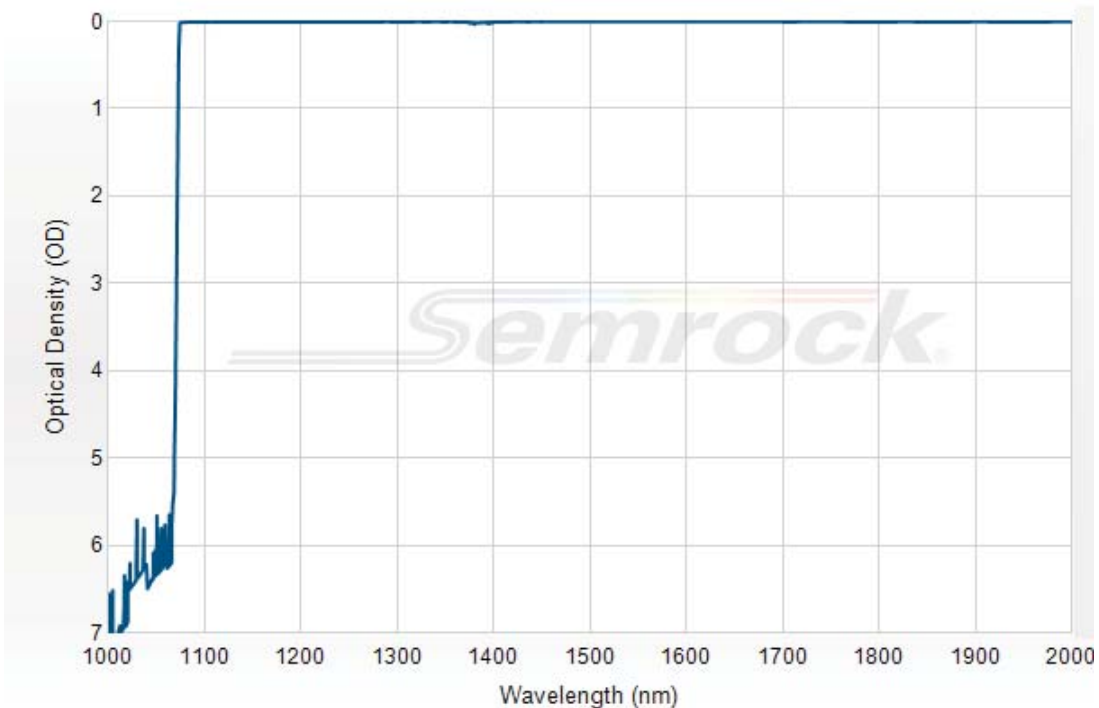


Figure 26: Transmission characteristic of the used long pass filter [19]

Applying the *Semrock* filter led to significant improvement in SNR, as it was expected.

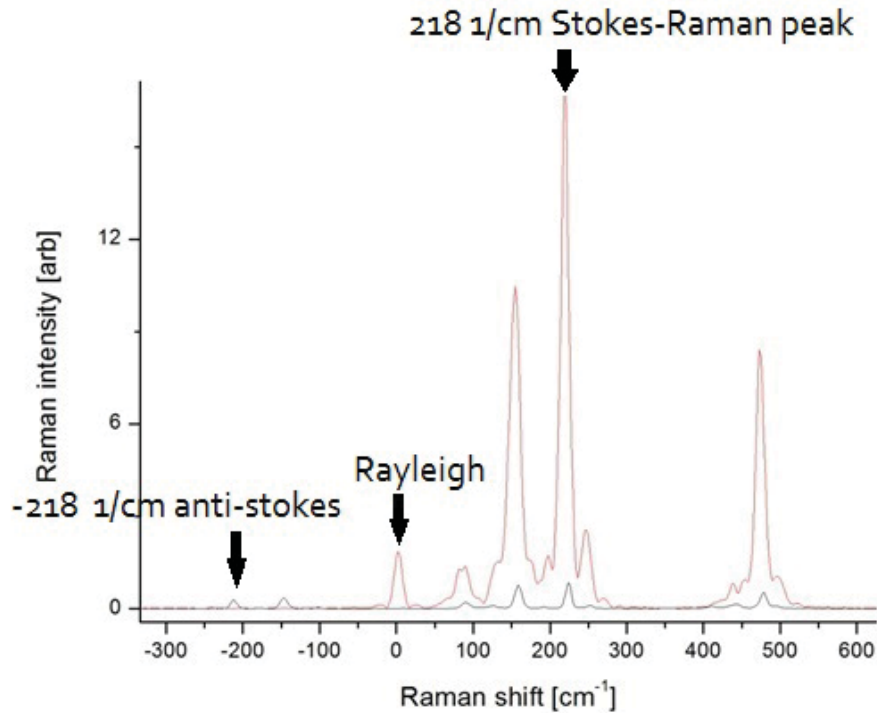


Figure 27: Black curve is the Raman spectrum of sulphur with the original setup. Red curve is the Raman spectrum of the same sample after applying the interference filter

The original (black) SNR was 170, by applying Semrock filter (Red) SNR became 1126 see Fig. 27, this means a factor of 6 compared to the Bruker's own filter, and factor of 3.75 compared to the best performance value in the Bruker's own benchmark for this type of spectrometer. Note that the Rayleigh light (R) became visible for the Semrock filter, whereas it is absent for the Bruker filter. Also note that the Semrock filter does not allow the observation of the anti-Stokes modes (AS).

The FT-Raman spectrometer contains a laser cleaning filter which removes unwanted bands from the NdYag laser, which would contaminate the Raman spectra. The original filter in the Bruker spectrometer had a transmission of 50% , which means that a substantial amount of laser power is wasted which requires a larger working current and thus a shortened laser lifetime. We removed this filter to inspect the unwanted bands and placed in a filter *1064 nm MaxLine laser clean-upfilter Part Number: LL01-1064-12.5* with a transmission of 96% in the passband. The role of the filter is to clean the Nd-YAG laser beam radiation of other than 1064 nm radiation, this improves the quality of the spectrum. The difference is well observed, the black curve is a spectrum without laser line filtering of Nd-YAG, which leads to additional peaks, faking the intensity of other peaks under same circumstances (85mW laser power).

The original Bruker spectrometer contained further optical elements in the path of the collected light: a planar mirror and a lens. All three were replaced by a single parabolic mirror *Thorlabs 2 inch 90° Off-Axis Parabolic Mirrors, Protected Aluminum*

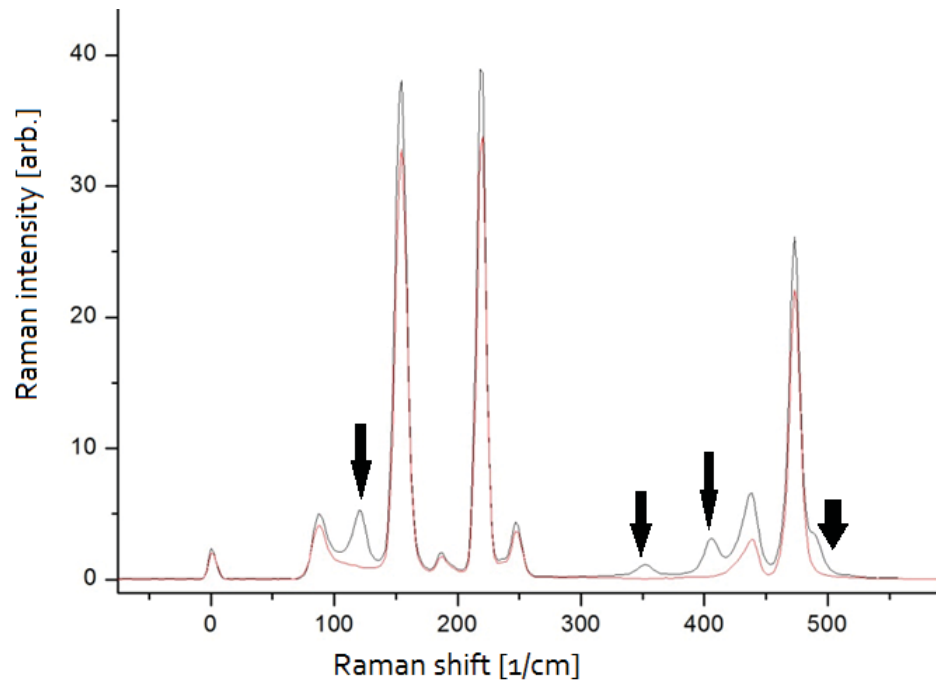


Figure 28: Red curve is the Raman spectrum of sulphur with the original setup. Black curve is the Raman spectrum of the same sample after applying the laser line filter. Peaks at 160cm^{-1} , 410cm^{-1} and 485cm^{-1} disappeared as shown by the arrows

Coating . This has the advantage of reducing the number of optical elements but also the replacement of a refractive element by a refractive, makes the setup inherently broadband. the optical path is shown Fig. 31 and Fig. 32. The mirror was mounted on a home manufactured bearer, that allowed moving the mirror in the x-y plane.

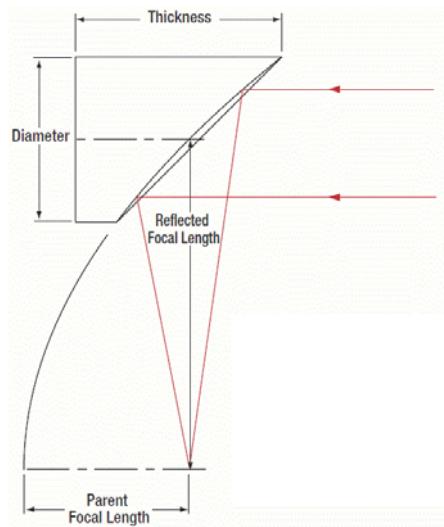


Figure 29: Schematics of the used off-axis parabolic mirror[20]

Type	90° Off-Axis
Diameter (mm)	50.8
Diameter Tolerance (mm)	+0.00/-0.38
Focal Length Tolerance (%)	±1
Surface Accuracy (λ)	1/4 RMS
Effective Focal Length EFL (mm)	101.60
Surface Roughness (Angstroms)	<175 RMS
Substrate	Aluminum 6061-T6
Coating	Protected Aluminum
Y Offset (mm)	101.60
RoHS	Exempt

Figure 30: Datasheet of the used parabolic mirror [20]

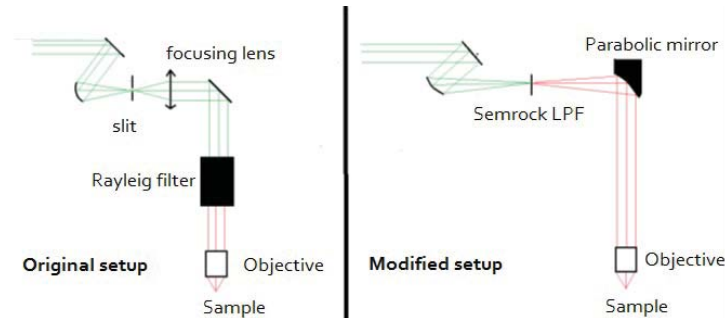


Figure 31: Schematic of the modified optical path of *IFS66V* spectrometer

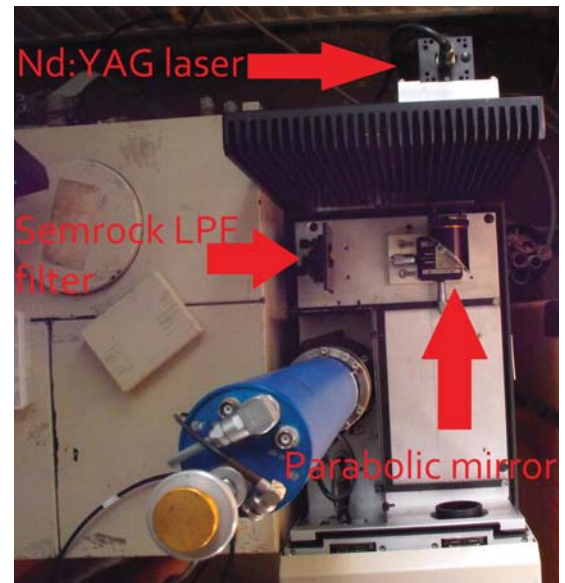


Figure 32: Photograph of the modified optical path of *IFS66V* spectrometer

We compared the performance of LPF with an commercial modern Bruker FT-Raman in the University of Vienna, the results are represented in Fig. 33. by taking a spectrum of the same sample, under the same measurement conditions and parameters The surplus peaks in the red spectrum is due to the lack of laser clean up filter. The applied LPF in our spectrometer did bring much difference in the SNR, as the one in Vienna has a Rayleigh filter with the same efficiency of *Semrock* filters. Due to the simplified optical, and better alignment, our spectrometer has a factor of 2 better optical throughput for the exciting laser and a 60% better SNR. The following table Fig. 34 summarizes the performance of the improved spectrometer in comparison to the manufacturer's benchmark, its original state and to that of a newer generation FT-Raman spectrometer at the University of Vienna.

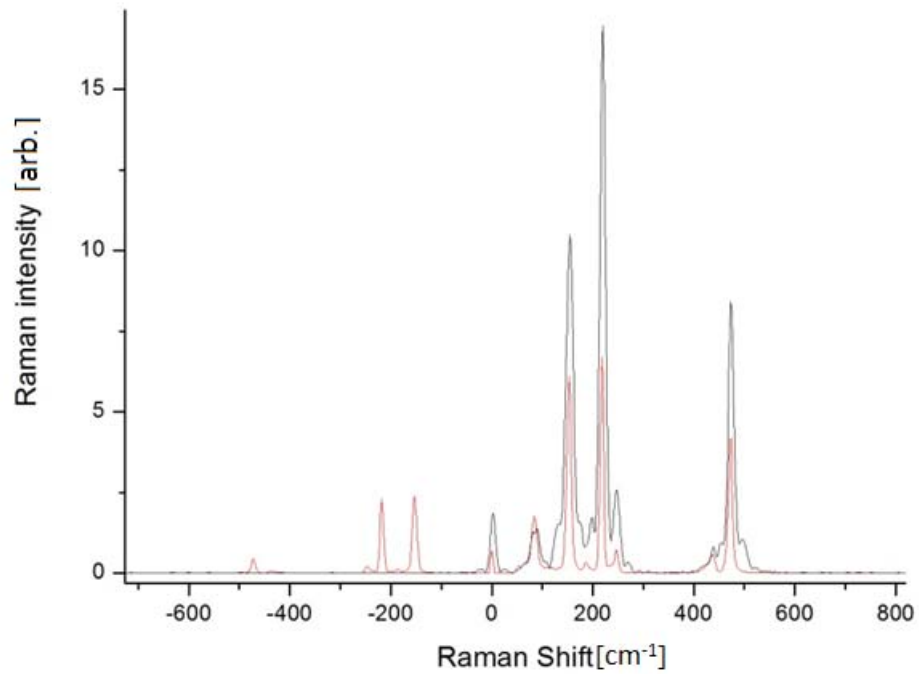


Figure 33: Red curve is the sulphur spectrum produced by a commercial spectrometer *Bruker RFS100/s* at the University of Vienna. Black is spectrum of the same sample under the same measurement conditions taken by or modified spectrometer.

stage of development	improvement	SNR
manufacturers benchmark	1 (reference)	300
delivery state	0.566	170
applying Semrock LPF	3.74	1120
spectrometer at Vienna	2.33	700

Figure 34: performance of the spectrometer compared to the original banchmark, and other spectrometers. The performance factor is relative to the manufacturers benchmark

As mentioned before, sulphur was chosen as reference sample because of its intense Raman peaks, which enabled the ease of monitoring the development and characterizing the spectrometer. The purpose at first place of the spectrometer is to investigate and characterize carbon nanotubes. Fig 35 shows Raman spectra of single wall carbon nanotube: NCG192 (Batch name of the sample), taken under 2 scans and 10 minutes (320 scans)with the upgraded spectrometer. We indicate in Fig. 35 that the most dominant Raman modes of SWCNTs: the Radial breathing mode around 200 cm^{-1} (RBM), the graphitic mode (G) around 1580 cm^{-1} and the so-called 2D mode around 2650 cm^{-1} . In summary, we have recovered a not functioning FT-Raman spectrometer and we have

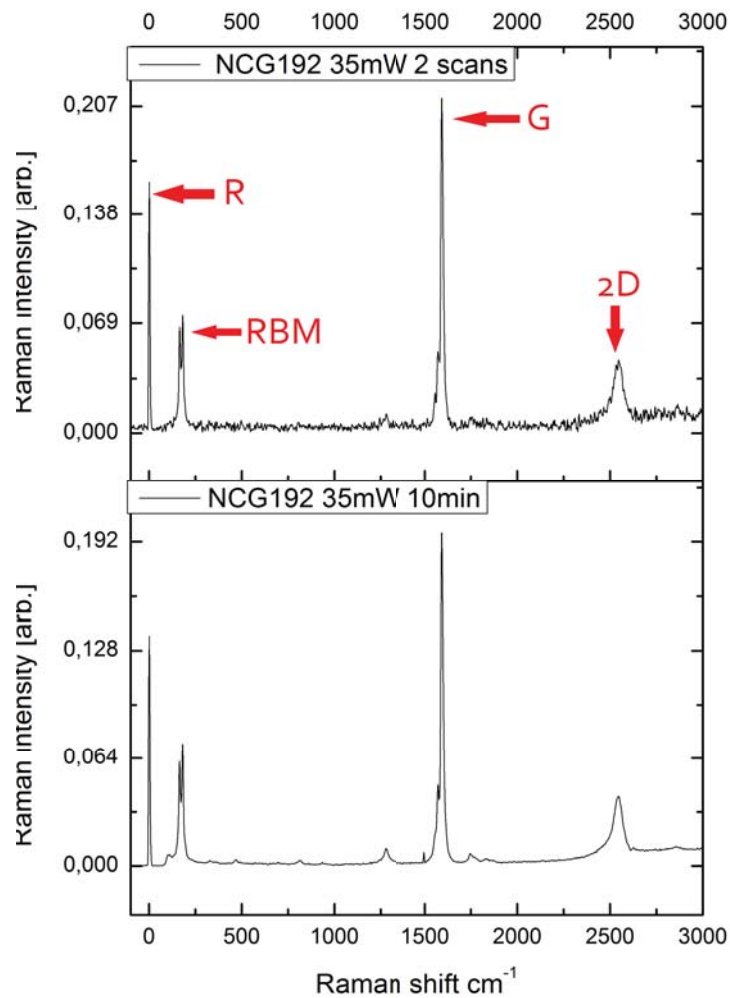


Figure 35: Raman spectra of SWCNT NCG192, upper spectrum was averaged from 2 scans, while lower spectrum was measured for 10 minutes (320 scans averaging)

substantially improved its optical properties in terms of sensitivity, simplicity and laser power.

4.2 Improvement of a microscope FT-Raman spectrometer

The *Bruker RFS100/S* FT-Raman spectrometer in the group of Prof. Thomas Pichler was a more modern version of the one discussed in the previous section. The major difference to the IFS66v is the presence of a NIR microscope which enables high spatial resolution as well as a well focused and intensive laser irradiation of samples. The interest came in the Pichler group to let their spectrometer be improved with the use of modern interference filters, too due to two reasons. First, it was assumed that insufficient laser power was reaching the samples under the microscope due to the non-optimal setup of irradiation. Second, it was assumed that similarly to the IFS66v, the light collection efficiency and thus the sensitivity could be improved. I overtook these goals during a summer internship in 2012.

4.2.1 Original state of the apparatus

As a first step, laser throughput of the system was determined by measuring the laser intensity just after the laser itself at the backside of the spectrometer, this is considered as the input power. Output power is the laser intensity on the sample in the microscope (Ramanscope) without an objective.

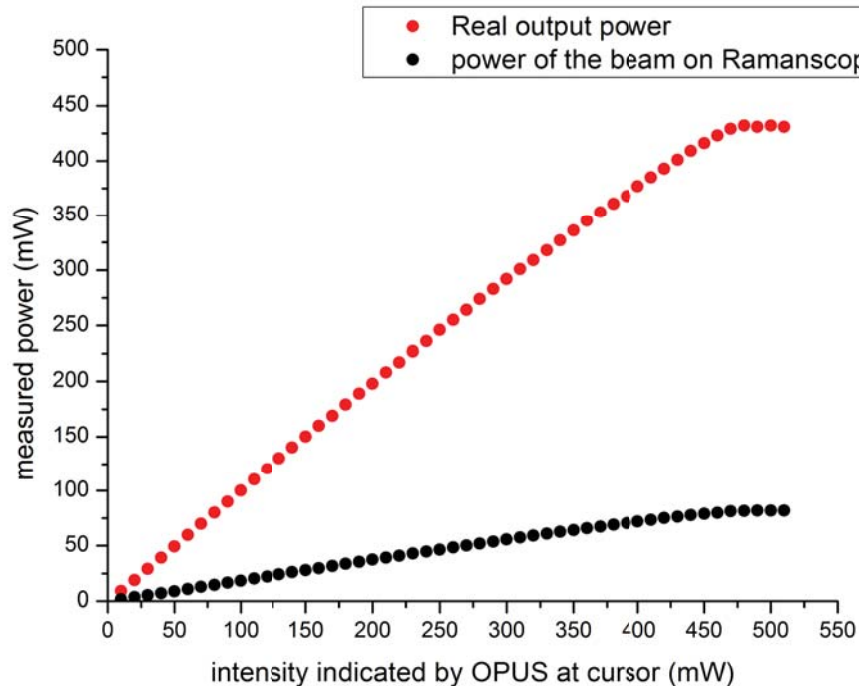


Figure 36: the measured real operating power (red) and output power (black) of the system with respect to power set in OPUS

The intensity of the laser is reduced by average 83%, that means only 17% of the power is present on the sample at any power level, see Fig. 36 .

As for the Raman collection efficiency SNR, was determined with 18 mW on a sulphur sample, using 10x objective (5 kHz mirror velocity and 4 cm^{-1} resolution). peak at 218 cm^{-1} is taken as signal, noise is taken from 3000 cm^{-1} to 1000 cm^{-1} like the previous studies Fig. 37. SNR was 186 in the original setup

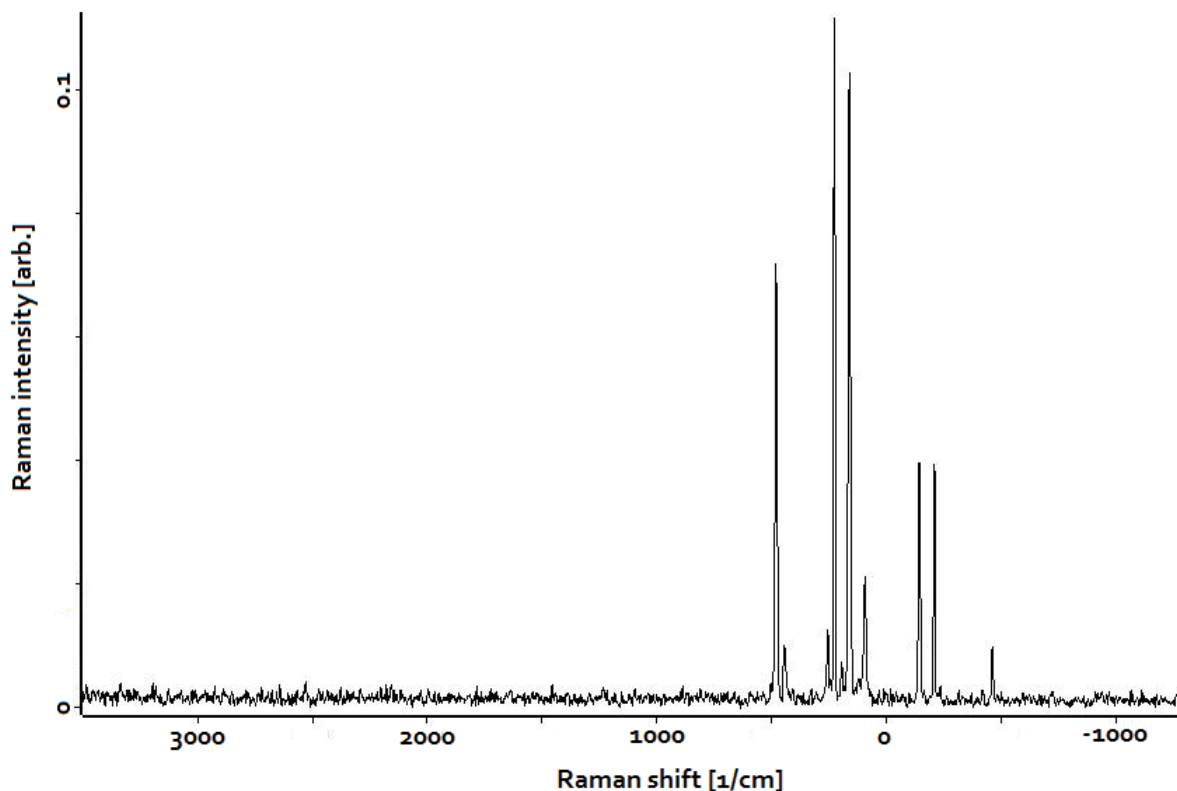


Figure 37: Sulphur spectrum of the microscope at 18mW incident power SNR = 186 in the original setup of the spectrometer

In the original configuration, laser was guided to the microscope by 3 mirrors, before entering the microscope. Inside the microscope the laser reached the sample through a relatively complicated optical path which serves as "optical duplexer", i.e. separates the excitation from the emission simultaneously via a series of mirrors, lenses and filters see Fig. 38. The poor laser line transmission was due to the combined optical losses of the elements. We note that, we could not clearly identify the type of the "Bruker 1064 colored filters" in Fig. 38. Their role is however to transmit the exciting light and to reflect the back reflected light. Our intensity loss measurements and the improvement itself proves, however that these filters are clearly inferior to the property of the Semrock interference filters.

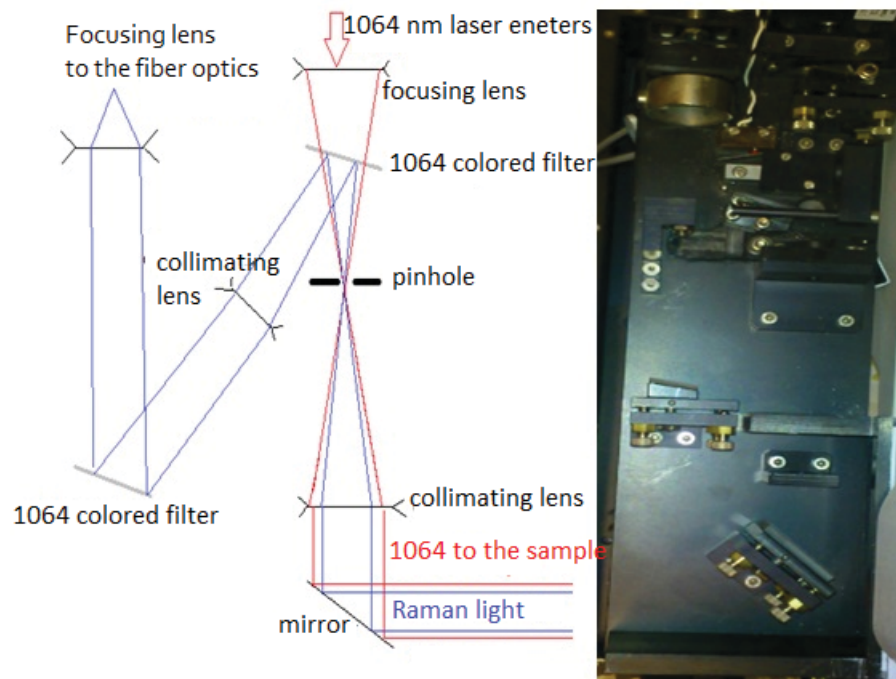


Figure 38: photo(right) and ray tracing schematics (left) of the collecting and laser guiding optical of the microscope of the original setup. Red is the 1064 nm laser, blue is the Raman light coming from the sample

This poorly designed configuration both decreases the laser power reaching the sample and the number of collected Raman photons. As described below, we have improved both with the use of modern interference filters.

4.2.2 Modifying the optical path

As a solution to the before mentioned problems, a periscope system was introduced as an optical coupling between the microscope and the spectrometer, as shown in Fig. 39 and Fig. 40

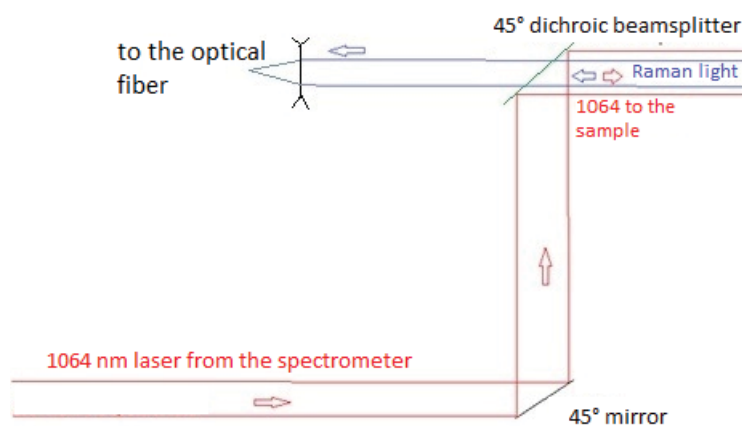


Figure 39: ray tracing schematics of the new collecting and laser guiding optical coupling of the microscope

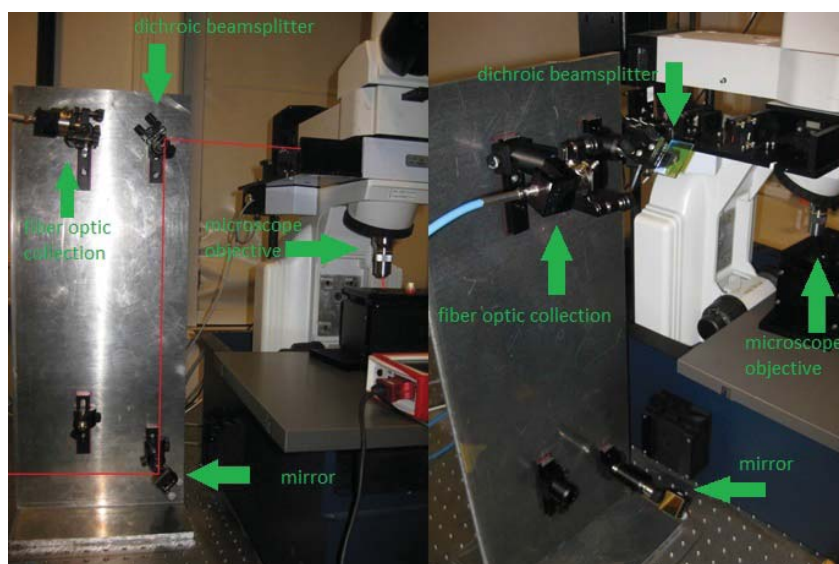


Figure 40: photo of the new collecting and laser guiding optical coupling of the microscope

The laser beam coming from the spectrometer is reflected by a mirror towards a dichroic beamsplitter (Mirrors used in the periscope are ME1S-M01 - 1" Square Protected Gold Mirror, 3.2 mm thick from *THORLABS* that have maximum reflection in the IR range). This is the critical part of the optical coupling, it is a *Semrock* 1064 nm long pass filter operating at an angle of incidence (AOI) of 45° (OD2 rejection). this reflects the exciting laser radiation towards the sample and transmits the Raman scattered photons coming from the sample. The transmitted photons are collected by an optical fiber system. Clearly, and this OD2 filter is appropriate for our purpose as only 1 % of the exciting laser is lost, whereas for the Raman light, it reduces the Rayleigh to one in a hundred. Certainly, additional Rayleigh filtering is required but it is provided by the built in Rayleigh filter of the spectrometer. Therefore this AOI 45° filter serves as the optical duplexer.

The transmission function of this filter is shown in Fig 35. in terms of optical density and percentage:

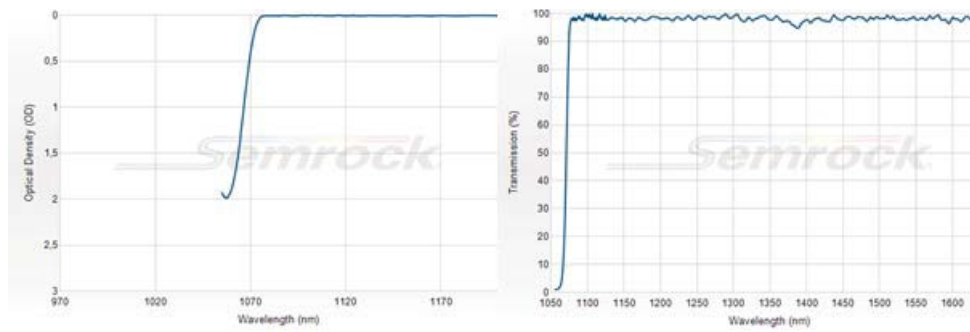


Figure 41: Transmission of the dichroic beamsplitter in % and OD with respect to wavelength [21]

The advantage of the periscope system are:

- significantly less optical elements which reduces optical losses
- the used *Semrock* filter is a high quality interference filter, which further improves the optical throughput
- simpler optical path makes optical alignment easier to carry out

Due to the introduction of the periscope coupling, intensity output improved by a factor of two.

Further improvement in the intensity output was achieved by replacing the laser's original clean up filter, by a *1064 nm MaxLine® Semrock laser clean-up filter Part Number: LL01-1064-12.5* that has a 96% transmittance of the laser line instead of 50% of the original built in filter. This improvement was essentially the same which we did previously for the IFS66v spectrometer in Budapest. This amounts to an additional factor of two improvement in the outgoing laser power. The achieved improvement is shown Fig. 42

The transmission of the periscope coupling and the new laser line filter is 66% instead of the original 18%, that means a factor of 3.5 gain in the laser power through-put.

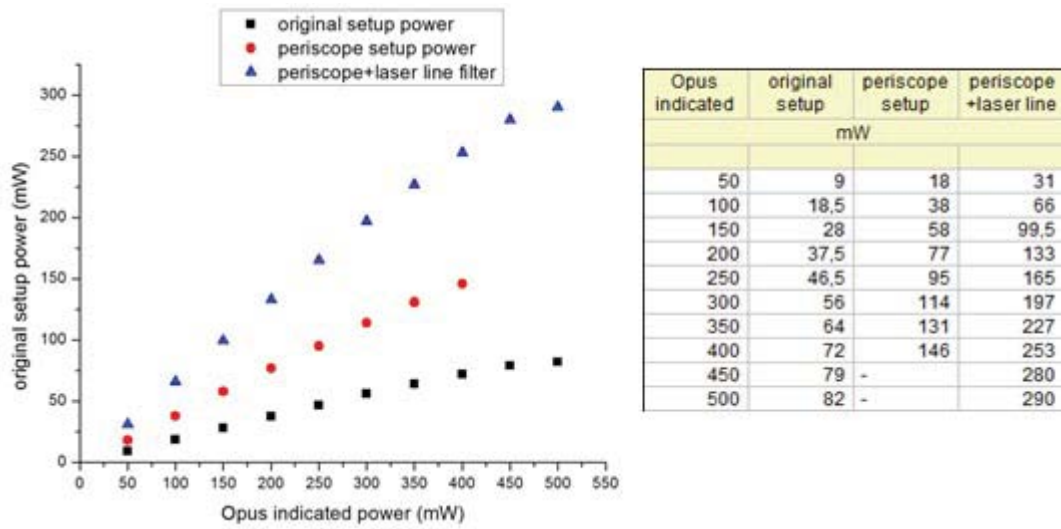


Figure 42: left: black points are the measured original output power, while red is the increase due to the periscope system, and blue the increase due to the periscope and the clean-up (laser line) filter. Right: the measurement results numerically.

4.2.3 Improvement in Raman photon collection efficiency

The improved optical path resulted in a simpler (i.e. with less optical elements) arrangement also for the Raman light collection. We decided to keep the optical fiber, as it has attenuation less than 10% and its coupling to the inside of the spectrometer was ready for use. Changing optical fiber coupling to lens system is complicated, as the system has to be corrected against optical aberration (spherical, chromatic, IR anti reflection).

We determined the improvement in the Raman light collection efficiency by our standard benchmark measurement on sulphur. signal to noise was calculated as follows:

Sample: Sulphur with 10x objective (yellow)

parameters:

power on sample	18mW
scannervelocity	5kHz
scans	2
resoulution	4cm ⁻¹

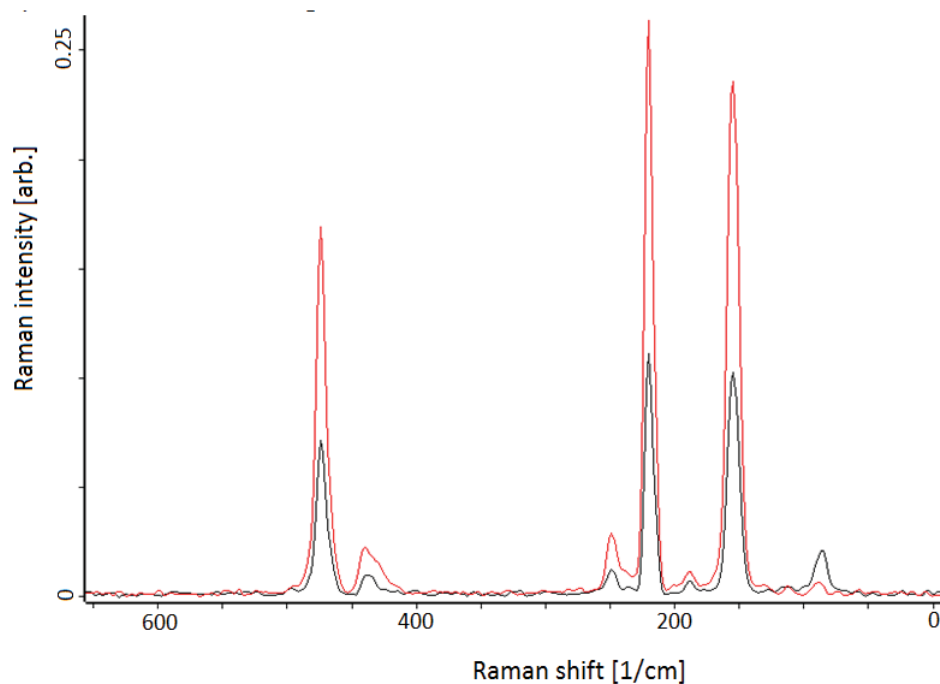


Figure 43: Spectrum of Sulphur before (black) and after (red) modification, with the same measurement parameters

peak at 218 cm⁻¹ is taken as signal, noise is taken from 3000 cm⁻¹ to 1000 cm⁻¹. Noise did not increase significantly (from 6 10⁻⁴ to 9 10⁻⁴) while signal got more than doubled (factor of 2,7), in total the improvement is a factor of 2 in collecting Raman signal Fig. 43.

4.2.4 Application of inverse beam expander

While installing the periscope setup we learned that the diameter of the laser beam is larger than the aperture of the microscope objectives, thus a substantial part of the laser beam was rejected and it never reaches the sample. In order to improve the laser transmittance of the optical coupling, it was necessary to shrink the laser beam. A beam expander was applied in inverse setup before the first mirror of the periscope, which is a standard Kepler telescope.

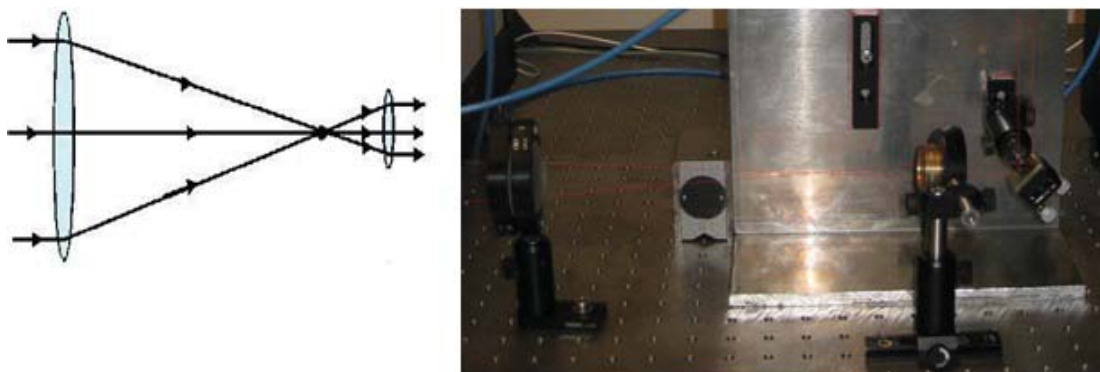


Figure 44: Standard Kepler telescope to reduce the diameter of a collimated beam.

Applying the Kepler telescope resulted in the decrease of the radius of the laser beam illuminating the sample. This was true only for two of the three used microscope objectives; objectives *Nikon LWD* and *Nikon LWD M* both of them have magnification factor of 40 while, as the third objective *Nikon 10X* with magnification factor of 10 had already wider entering aperture than of the unshrunk laser beam, in this case no increase in the excitation was observed while using this objective.

The result of the modification is showed below in a table, power at the sample of the original setup (without beam expander) is compared to the application of the beam expander. The improved laser throughput was measured and shown in Fig. 42 :

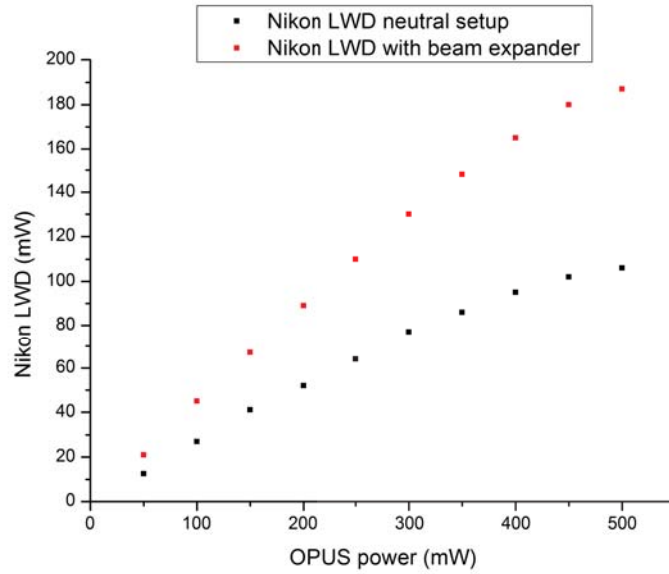


Figure 45: The output power as function of laser power of objective *Nikon LWD*(Magnification:40) without- (black) and with (red) beamsrinker . 65% improvement is observed due to the beamsrinker.

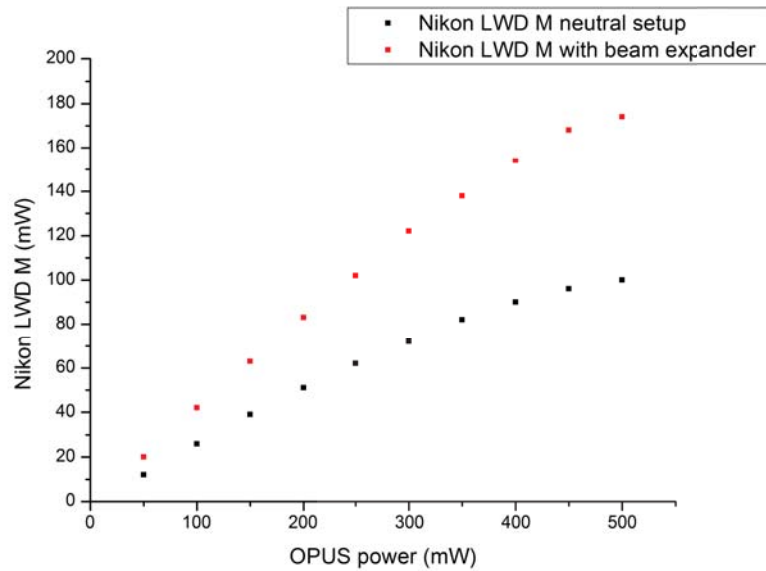


Figure 46: The output power as function of laser power of objective *Nikon LWD M*(Magnification:40) without- (black) and with (red) beamsrinker . 65% improvement is observed due to the beamsrinker.

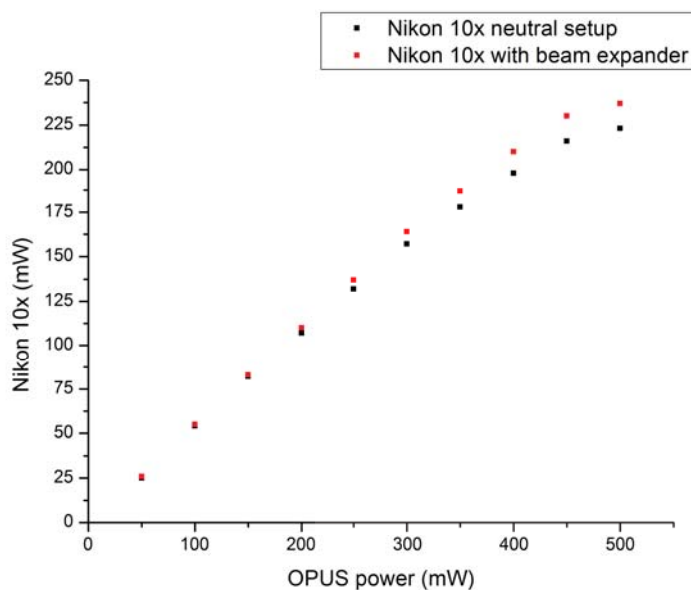


Figure 47: The output power as function of laser power of objective *Nikon 10X*(Magnification:10) without- (black) and with (red) beamsrinker . No significant improvement is observed due to the beamsrinker, as the aperture of the objective was already bigger than of the unshrunked incident light

The transmission increased by average 65% in case of Nikon LWD and LWD M objectives , while only a few percent in case of 10x objective. Both LWD and LWD M objectives have small aperture, while 10x objective has big aperture to fit unshrunked beam.

In summary, we have improved the FT-Raman spectrometer at the University of Vienna by redesigning both the optical excitation and emission paths. The most important element was a AOI 45° interference filter which acts as an optical duplexer. The exciting laser intensity was increased by a factor of 4-6 (depending on the objective type) using modern filters and a beam shrinker. The Raman light collection efficiency was improved by a factor 2.7 . Overall, per a given Nd-YAG laser driving current, we have improved the spectrometer performance by a factor of 10, which gives shorter acquisition times and increases the laser lifespan.

4.3 Development of a visible FT-Raman spectrometer

In the following I demonstrate the construction of VIS-FT Raman spectrometer by means of carrying out modifications on a *Bruker IFS 66v* FT-IR spectrometer. I show the procedure of building the optical setup of such spectrometers, and the corresponding detector system. As it was mentioned in Chapter 2., the common sense dictates, that visible FT-Raman spectrometers do not function as well as their NIR counterparts. We would like to explore this by our own means and with the knowledge gained in the spectrometer development.

4.3.1 The optical configuration of VIS FT-Raman spectrometer

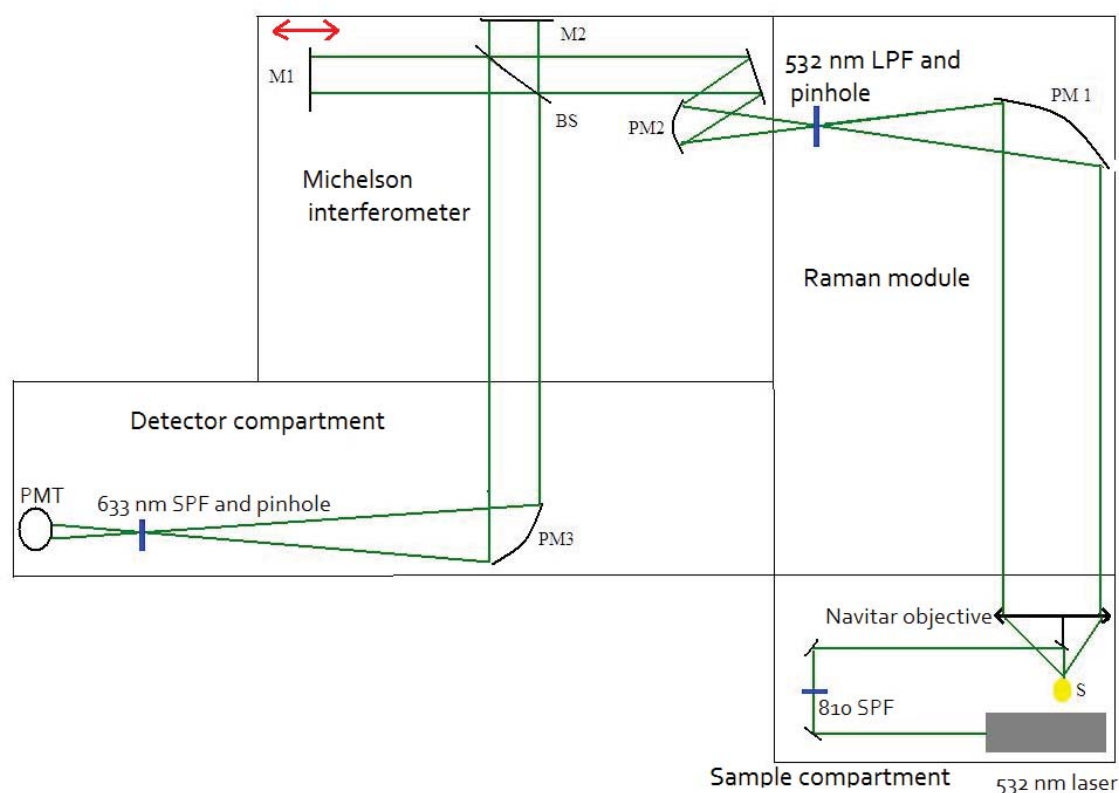


Figure 48: The optical setup of VIS-FT Raman spectrometer

For Raman spectrometer in the visible range, the NIR FT-Raman spectrometer had to be rebuilt. This involved changing the excitation, optic guiding and detection elements.

In the sample compartment see Fig.[48] a 532nm frequency doubled Nd:YAG laser was installed as light source. The light beam passes through a 810nm short pass filter (SPF) as the Nd:YAG crystal is pumped with a diode laser working around 808-810 nm, thus the 532 nm laser radiates a non-negligible amount of this light. This wavelength, if

unfiltered, enters the spectrometer and contributes to the noise level (see later). Laser light is guided to the sample (S) with two dielectric mirror and a small (3x3 mm) 90 degree prism mirror. Raman photons are collected with a *Navitar – DO5095* camera objective, that has $f/\# = 0.95$ f-number, It is based on the so-called double Gaussian lens principle i.e. it is corrected for both spherical and chromatic aberration and has $D = 31\text{ mm}$ open aperture. This is essentially the smallest f-number (also called a "fast lens") objective, which is available commercially. The sample is placed in it focus and the output parallel beam is focused by a parabolic mirror (PM1) to a 532nm long pass filter (LPF) that has $OD7$ rejection to filter out Rayleigh radiation. We found that a pinhole with about 2 mm diameter behind the LPF decreases substantially the level of the Rayleigh radiation. Interestingly, if the pinhole is in front of the filter, the performance is inferior, as the LPF illuminates the back of the pinhole, and the scattered light from the pinhole insides with a big angle of incidence (AOI), penetrating the filter. The beam is introduced to the Michelson interferometer with a *Bruker T502/1* Quartz beam splitter (BS), This is the standard VIS BS of the Bruker instrument optimized for 833 nm to 470 nm The modulated light is focused with PM3 on a 633nm SPF that filters out the light from the He-Ne laser (which is the control laser of the interferometer). Eventually, the interferogram is detected with a *Hamamatsu: R955* photomultiplier tube (PMT).

4.3.2 Electronic configuration

The use of oscilloscope to monitor the interferogram is necessary because the spectrometer has a built in DC filter see Fig. 49 50. As DC signal corresponds to the part of the light that does not participate in the interferogram. Its amount is indicative to what extent the interferometer is well aligned: if the alignment is bad the DC level is large. Ideally, the DC level is zero and the interferogram is maximal, this is the so-called fringe visibility. It is vital to measure it, because although it dose not correspond to Raman signal, but it does enhance noise (see later).



Figure 49: detector signal displayed on oscilloscope allow to measure the DC signal component of the detected light

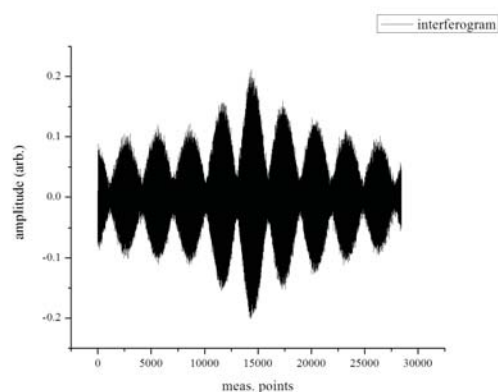


Figure 50: Digitalized and displayed signal of the PMT which is detected with the Bruker IFS66v. It is free of a DC component.

4.3.3 The signal-to-noise performance

The electronic conversion factor

In order to properly characterize the performance of the VIS FT-Raman spectrometer, we measured some characteristics of the spectrometer electronics itself. The scale factor between the input signal and that displayed by the OPUS software was measured first. To do so, we connected a 1V peak to peak sine AC voltage to the detector input slot of the spectrometer, the result is shown in the following table:

Absolute voltage	peak to peak signal in the interferogram	amplitude of the corresponding peak in the spectrum
1 V	0.1 opus units	3 opus units

This means that for a $1V_{pp}$ AC signal the spectrum will be a 3 opus unit high peak. Besides, we also learnt that the A/D converter of the spectrometer saturates for a 20 Vpp signal at 1 opus units, which is displayed as 32768 counts.

The shot noise

The main noise source in NIR and VIS spectroscopy are different. NIR spectroscopy is detector noise limited due to the relatively inferior quality of infrared photodiodes. The density of the thermally excited electrons in the conduction band follows the Fermi-Dirac statistics in the applied photodiode, the thermal noise dependence of gap magnitude is a very strong exponential decay. For the NIR regime (typical energy of 0.8 eV - 1.2 eV) there is a considerable thermal noise, while in VIS regime(2.3 eV) there is negligible thermal noise (this is why NIR photo diodes are usually cooled, while VIS photodiodes work at room temperature).

VIS spectroscopy is usually shot noise limited. Shot noise arises due to the quantized nature of light. Walter Schottky discovered in 1918 that the quantized nature of light gives rise to a noise of:

$$\sqrt{\langle(\Delta I)^2\rangle} = \sqrt{\langle I\rangle 2e\Delta f} \quad (17)$$

Where I is the induced photocurrent. Eq. 17 and 29 also describes the spectral power density of the shot noise

$$S_{Shotnoise}(f) = \frac{\langle(\Delta I)^2\rangle}{\Delta f} = 2e\langle I\rangle \quad (18)$$

Eq. 18 and 17 tells two very important things about shot noise:

1. Shot noise of the PMT signal increases with the square root of the incident power and the bandwidth (Δf), Noise $\sim \sqrt{P}$ or $\sqrt{\Delta f}$.
2. Shot noise spreads across the whole spectrum evenly forming a *white noise*,

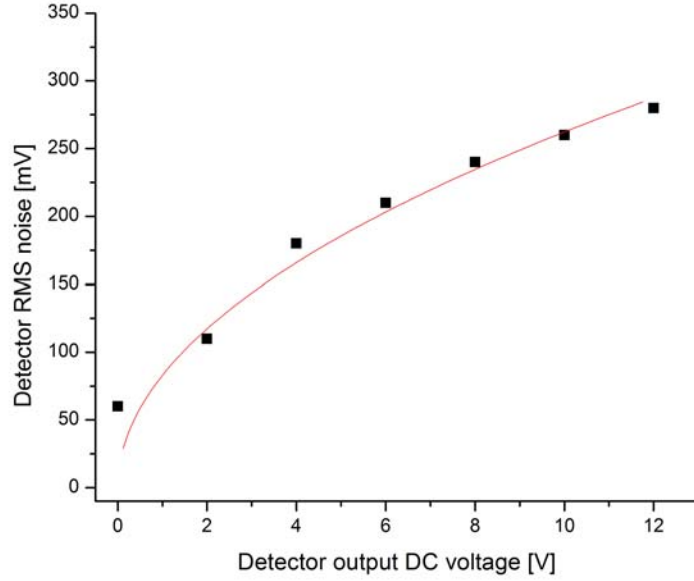


Figure 51: The RMS noise of the PMT for different output voltage achieved by varying laser intensity. The red line is a square root function fit to the measured points

Point 1. was measured by varying the laser power, the output DC voltage of the detector was monitored with an oscilloscope while a RMS noise was measured Fig. 51. It can be seen from Fig 51. that the noise dependence of the light intensity is in a good agreement with the \sqrt{P} expected dependence for high power, but for weak power the main noise is thermal noise. This dependence is further confirmed by the following measurement, where the PMT was irradiated with constant light intensity produced by the built in halogen lamp that has a broad band black body radiation. The noise was evaluated from the spectrum and also measured with an oscilloscope. The consistency of the shot noise nature of noise was performed by a comparison between a measurement and calculation as follows.:

The PMT supply voltage U_s was adjusted until the output signal corresponding to the power of the light coming from the NIR source reached $U_{output} = 10V$ that corresponds to $U_s = 530V$ supply voltage, that further corresponds to PMT gain factor $G = 6 * 10^4$ see Fig 22. The I/V converter gain was set to $g = 10^5 \frac{V}{A}$, measurement with the oscilloscope was carried out with $20kHz$ BW ($BW = \Delta f$).

The evaluated noise was $V_{RMS} = 20mV$ from the oscilloscope measurement. The noise was calculated as follows:

$$\begin{aligned}
I_a &= \frac{U_{PMT}}{g} = 10V * 10^{-5} \frac{A}{V} = 10^{-4} A \\
I_c &= \frac{I_a}{G} = 10^{-4} A * \frac{10^{-4}}{6} = 1.7 * 10^{-9} A \\
I_{noise,c} &= \sqrt{2 e I_c \Delta f} = 1.64 * 10^{-12} A \\
I_{noise,a} &= I_{noise,c} * G = 9.84 * 10^{-8} \\
V_{RMS} &= I_{noise,a} * g = 10mV
\end{aligned} \tag{19}$$

Where I_a is the anode- and I_c is the cathode current. Calculated RMS noise based on estimation yielded $V_{RMS} = 10mV$, while measurements yielded $V_{RMS} = 20mV$, which are in good agreement.

The conclusion is that based on Fig. 51 and calculation Eq. 20 the noise observed in our experiment is shot noise dominated. This also means that there is no need to cool the PMT as it would only reduce the shot noise contribution from the dark current, which is orders of magnitude smaller than the signal related shot noise. Another consequence of the shot noise nature of the noise, is that the two ways to gain signal to noise is to i) suppress unwanted background light, ii) increase the optical throughput of the spectrometer. The latter yields a square root improvement in the SNR, while for a NIR detector the improvement of SNR goes linearly with the intensity of the detected light.

4.3.4 The signal

After we completed the optical setup mentioned in the previous section, a Raman spectrum of sulphur was acquired. Fig 52 and 53 shows the recorded interferogram and the spectrum. We chose sulphur repeatedly because of the strong Raman peaks, and the lack of fluorescence and thermal background of the sample.

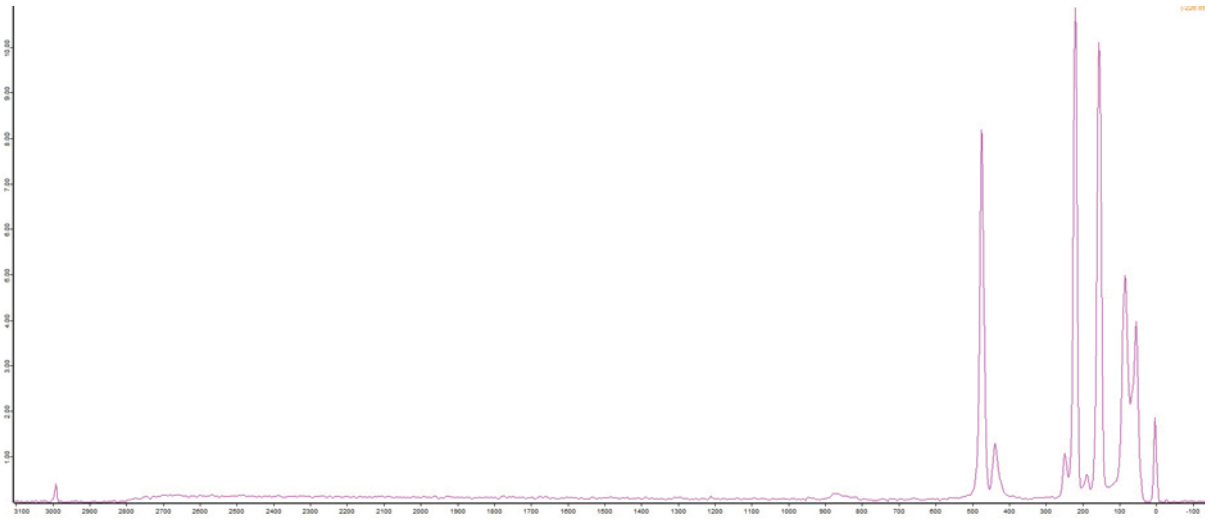


Figure 52: Recorded sulphur spectrum with VIS-FT Raman spectrometer

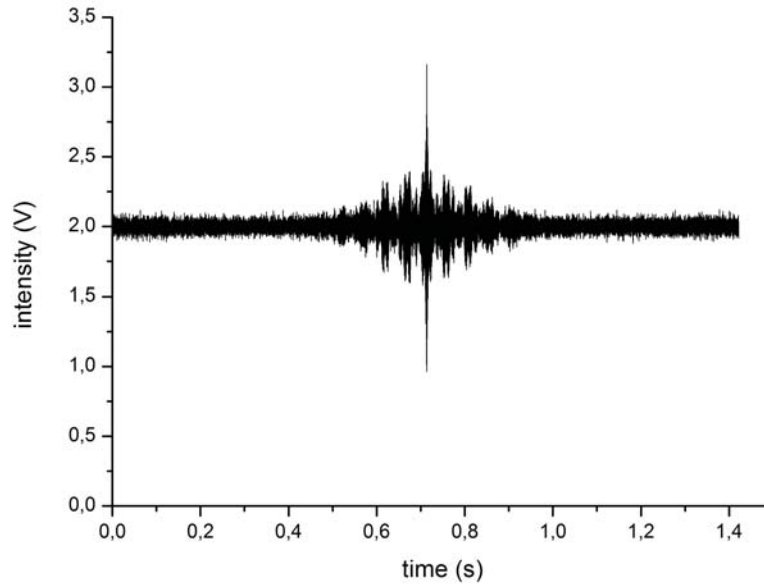


Figure 53: Recorded sulphur interferogram with VIS-FT Raman spectrometer

The spectrum was acquired with $5kHz$ bandwidth for 60 seconds until which 38 double sided (forward-backward mode see chapter 1) scans were acquired. Signal to noise ratio of the spectrum is $SNR = 470$.

As mentioned in the previous section, the main source is shot noise, which depends linearly of the square root of the detected light power, thus it is critical to suppress any incident light other than Raman. In the case of our home-built VIS-FT Raman, three main light sources were identified that contribute vastly to the noise besides the Raman scattered photons.

1. Rayleigh peak

This is the most intense radiation in the spectrum, thus it is the most critical part of the optical setup to filter out the Rayleigh peak. Using good quality interference filters the problem can be fixed.

2. Uniform background

It is critical for the interferometer to be aligned properly so the two beams coming from the two mirrors exit the interferometer collimated and parallel, if this condition is not met, then a part of the light entering the interferometer does not interfere with itself. As mentioned in the theoretical introduction, interference of two light sources only occurs when they are coherent. The emitted Rayleigh and Raman photons have short coherence length, therefore the *Zero Path Difference* (ZPD) of the spectrometer has to be set properly. This effect can be reduced by setting the interferometer to sweep symmetrically with respect to the point or ZPD.

3. Broadband radiation Broad band radiation can appear due to the photo luminescence-

or black body radiation response of the sample to the laser radiation. Or even background light can enter the spectrometer. Unfortunately this effect can not be suppressed and depends on the sample. This is the main reason why FT technique is not popular in visible Raman spectroscopy.

In case of the measured sulphur spectrum there is no broadband background radiation. The measured fringe visibility yields that amplitude of the uniform background light detected at our best optical alignment is similar to that of the peak to peak amplitude of the interferogram see Fig. 53, meaning that the main contribution to the shot noise is due to the uniform background.

In the following, we prove that the spectrometer essentially detects all available photons, and the losses are compatible with the few optical elements with no considerable losses. Sulphur Raman spectrum was measured, with $10mW$ laser intensity, and $U_s = 800V$ PMT supply voltage. The detected absolute power of Rayleigh radiation was determined by measuring the Rayleigh peak intensity (the conversion factor between opus's arbitrary units of opus and the PMT signal is known from the table in the previous section). Using a conventional *Thorlabs* powermeter, scattered light power was also measured at the entrance of the PMT without Rayleigh filter. Knowing the Rayleigh attenuation factor of the filter and parameters of the PMT, we calculated the expected Rayleigh power and it was compared to the result gained from the measured result.

The measured unfiltered Rayleigh was $P_R = 30\mu W$, attenuation of the filter is OD 6.75, cathode radiant sensitivity $CRS = 60mA/W$ at $532nm$, PMT gain is $G = 2 * 10^6$, the I/V converter gain is $g = 10^5 V/A$

$$\begin{aligned}
 P_R &= 30\mu W * OD6.75 = 5.410^{-12} W \\
 \text{Cathode current : } I_c &= P_R * CRS = 3.24 * 10^{-13} A \\
 \text{Anode current } I_a &= G * I_c = 6.48 * 10^{-7} A \\
 \text{PMT output voltage } U_{PMT} &= g * I_a = 64.8; mV
 \end{aligned}
 \tag{20}$$

The measured light intensity in the spectrum was $P_R = 0.2 opusunits$ which corresponds to $U_{PMT} = 66mV$. The good agreement between the measured and calculated U_{PMT} values shows that the spectrometer detects the photons very efficiently.

4.3.5 Quality of the spectrometer

The main reason why FT technique was never popular in visible spectroscopy (or generally in shot noise limited measurements) is that the shot noise would degrade the multiplex advantage, which can be understood with the following consideration:

Suppose we want to measure a broadband spectrum eg. photo luminescence or absorption spectrum with a dispersive spectrometer, where the number of the measured points are N , and the integration time is τ , thus the measurement time will be $T = N * \tau$. Suppose we measure a total of M photons per unit time and in one measurement point the average of the measured photons is M/N . The noise will be proportional to the

square root of the measured photons i.e. $Noise \sim \sqrt{\frac{M}{N}}$.

As for FT spectrometer, the total number of photons M is measured simultaneously i.e. $Noise \sim \sqrt{M}$ but applying the same integration time N , spectra can be acquired during a measurement time of T , thus the noise is reduced by a factor of \sqrt{N} (multiplex advantage) meaning for T time $Noise \sim \sqrt{\frac{M}{N}}$. We can see that in a shot noise limited case FT technique loses the multiplex advantage, and not only this advantage is lost but because noise is spread all over the spectrum, weak details are hidden. This is the main reason why FT was never popular in the first place. This consideration tells us that FT spectrometers are inadequate for measuring weak Raman peaks located on an intense broadband luminescent background.

The most important question was how to quantify the quality of our spectrometer. The spectra measured with VIS-FT Raman spectrometer was compared with spectra acquired with a *Jobin Yvon 320 (JY320)* commercial single channel dispersive spectrometer, and the *Fellget factor* F is determined which is defined the signal to noise of the FT spectrometer divided by the signal to noise of the dispersive : $F = \frac{SNR_{FT}}{SNR_{disp}}$. The same

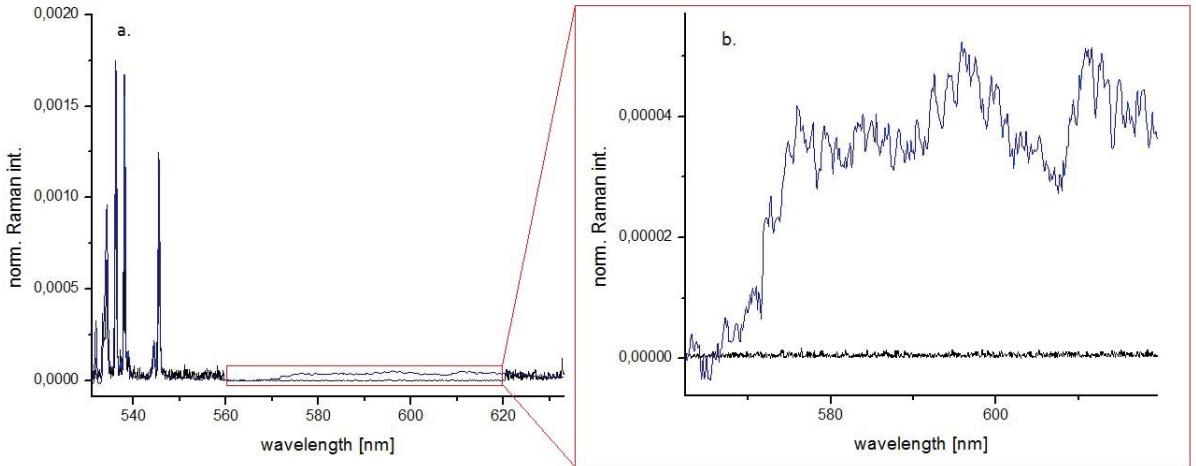


Figure 54: Fig. a. shows sulphur spectrum acquired with JY320 spectrometer (blue), measurement was taken for 5 minutes. black spectrum was taken with VIS-FT-Raman spectrometer for 0.8 s Fig. b. black curve shows the noise of FT spectrometer if for a measurement taken for 5 minutes while blue curve shows the noise of JY320 spectrometer

sample, electronics, laser and collecting objective was used in both measurements. The sample was illuminated with 10 mW laser power. Fig. 54 shows both spectra, spectrum taken with JY320 was acquired for 300 seconds, while FT spectrum was acquired by recording one one-sided interferogram for 0.8 seconds. if measured for 300 seconds, FT spectrometer would acquire 380 interferograms, which reduces the noise by factor of $\sqrt{380}$. The Fellget factor turned out to be $F = 10$, thus the signal to noise ratio of our VIS-FT Raman spectrometer is superior by a factor of ten to a single channel commercial dispersive spectrometer.

Summarizing this section, we have successfully modified the NIR FT-Raman spectrometer to enable measurements in the visible range. We have characterized the overall performance and have identified the noise source. We argued that this spectrometer can be competitive to dispersive instruments for the visible range.

5 Summary and outlook

Due to the application of thin film interference filters for Rayleigh filtering and laser line cleaning, along with the simplified and well aligned optical path, *Bruker IFS66v* FT-IR Raman spectrometer performance was considerably enhanced both for optical throughput and signal to noise ratio. The performance of the spectrometer shows a factor of 3.7 better SNR compared to the manufacturers benchmark data and a factor of 2.33 compared to a modern commercial spectrometer of the same manufacturer. Due to the simplified optical path, the spectrometer can be aligned much easier and it also paves the way for a broadband or a multi laser operation..

The confocal NIR Raman microscope system in the University of Vienna was improved. Applying the periscope system with a dichroic beam splitter, the Semrock laser clean-up filter and the inverse beam expander, we reached 66% instead of 18% transmission of the laser intensity, that means a factor of 3.5 improvement in the laser throughput, above this further 65% laser intensity improvement was gained on other objectives. A factor of 2 was gained in the signal to noise ratio, which would decrease the measurement time by factor of four to get the same spectrum. The new optical setup extended the lifetime of the laser and made annealing possible up to 237 mW with the 10x objective and 180 mW with the other two objectives (292 mW with no objective)

Bruker IFS66v spectrometer was rebuilt to operate in the visible regime. The setup of the necessary light source, optical guiding and detector elements was discussed. The primary noise source of the measurement was understood along with the consistency of the expected Raman signals and noise level. A comparison was made with a single channel dispersive spectrometer, the results showed that in our reconfigured spectrometer has a factor of ten better SNR than the dispersive one.

References

- [1] T. Hirschfeld and B. Chase. Ft-raman spectroscopy: Development and justification. *Applied Spectroscopy*, 40:133–137, 1986.
- [2] P. N. N. Laboratory. Raman scattering. http://www.doitpoms.ac.uk/tlplib/raman/raman_scattering.php, June 2007.
- [3] Hans Kuzmany. *Solid-State Spectroscopy: An Introduction*. Vienna Austria: Springer.
- [4] Stratingh Institute for Chemistry University of Groningen Netherlands Dr. Wesley Browne, Centre for Systems Chemistry. Raman in nir. <http://www.andor.com/learning-academy/raman-in-nir-ingaas-detector-and-swir-spectroscopy>, 2003.
- [5] Bob Mellish. Chromatic aberration lens diagram. http://en.wikipedia.org/wiki/File:Chromatic_abberation_lens_diagram.svg, March 2006.
- [6] Mglg. Spherical aberration. http://en.wikipedia.org/wiki/File:Spherical_aberration_2.svg, August 2006.
- [7] Erdei Gábor. *Egyetemi Jegyzet: Optika Fizika BSc III*.
- [8] J. Partanen J. Kauppinen. *Fourier Transform in Spectroscopy*. Wiley-VCH Verlag GmbH, 2001.
- [9] Eric W. Weisstein. Michelson interferometer. <http://scienceworld.wolfram.com/physics/MichelsonInterferometer.html>, 1996-2007.
- [10] F. E. Lytle. Even rectangle and sinc function. <http://www.chem.purdue.edu/courses/chm621/text/ft/basiset/rect/rect.htm>, 2001.
- [11] Siegfried Wartewig. *IR and Raman Spectroscopy: Fundamental Processing*. Wiley-VCH Verlag GmbH, Weinheim, 2003.
- [12] Travis Wakefield Christopher Hardee, Roy Kinoshita, 210 Main Street Brattleboro Vermont 05301. Turan Erdogan Semrock Inc. 3625 Buffalo Road Rochester New York 14624. Kenneth R. Spring Scientific Consultant Lusby Maryland 20657. Thomas J. Fellers Robert Johnson Omega Optical, Inc., and The Florida State University Tallahassee Florida 32310. Michael W. Davidson National High Magnetic Field Laboratory, 1800 East Paul Dirac Dr. Interference filters for fluorescence microscopy. <http://www.olympusmicro.com/primer/techniques/confocal/interferencefilters.html>, 2012.
- [13] Thorlabs. Interference filters for fluorescence microscopy. http://www.thorlabs.de/NewGroupPage9.cfm?ObjectGroup_ID=918, 2012.
- [14] Bruker. Digitect detectors. http://pdf.directindustry.com/pdf/bruker-optics/digitect-detectors/57234-264921-_2.html, 2013.
- [15] K. Rajagopal. *Engineering Physics*. PHI Learning Pvt. New Delhi.

- [16] Michael W. Davidson Mortimer Abramowitz. Concepts in digital imaging technology: Photomultiplier tubes. <http://learn.hamamatsu.com/articles/photomultipliers.html>, 2012.
- [17] HAMAMATSU. Amplifier unit c7319. <http://www.hamamatsu.com/jp/en/product/category/3100/3004/3049/C7319/index.html>, 2012.
- [18] Hamamatsu Inc. R955 photomultiplier tube datasheet. http://www.hamamatsu.com/resources/pdf/etd/R928_R955_TPMS1001E07.pdf, 2006.
- [19] Semrock Inc. 1064 nm razoredge® ultrastep long-pass edge filter part number: Lp02-1064ru-25. <http://www.semrock.com/FilterDetails.aspx?id=LPO2-1064RU-25>, 2011.
- [20] Thorlabs. Off-axis parabolic mirrors, protected aluminum coating. http://www.thorlabs.com/NewGroupPage9.cfm?ObjectGroup_ID=7003, 2003.
- [21] Semrock Inc. 1064 nm razoredge dichroic™ laser-flat beamsplitter part number: Lpd01-1064rs-25. <http://www.semrock.com/FilterDetails.aspx?id=LPD01-1064RS-25>, 2011.

Appendix

A Central Limit Theorem

$$\lim_{n \rightarrow \infty} P \left(\frac{\sum_{i=1}^n \frac{X_i}{n} - \mu}{\frac{\sigma}{\sqrt{n}}} > a \right) \rightarrow \phi(a) \quad (21)$$

Where X_i is the value of the $X_i - th$ measurement μ and σ are the expectance value and variance of the $X_i th$ measurement, this means that the value of the average over n measurements will tend to normal (Gaussian) distribution Φ as we average more and more. To comprehend this let us make the following experiment: let us measure with the detector no signal for t_0 time, obviously we will detect some noise, with 0 expectance value and σ variance (eg. thermal noise of the detector), let us repeat the measurement for $t_1 = 2t_0$, both measurements where sampled with the same sampling rate that is we have N measurement points from the first measurement and $2N$ from the second. Now let us make a histogram, x-axis denotes the value of a measured point, y-axis the number of points that yielded this value. Both graphs will tend to a Gaussian graph centered at 0, but the first will have $2.35 * \sigma_0 = 2.35 * \frac{\sigma}{\sqrt{N}}$ *FWHM* (Full Width at Half Maximum), and the second will have $\sigma_0 = \frac{\sigma}{\sqrt{2N}}$ according to the CLT. If we define the noise level P_{noise} of a measurement as the *FWHM* of this histogram, and we now repeat the two measurement but now with a given signal level at the detector the SNR of the second measurement will be $\sqrt{2}$ time SNR of the first measurement, that is if we conduct a measurement for time t than $SNR \sim \frac{1}{\sqrt{t}}$

B Fourier transformation and the FFT

In order to learn the know-how of FT-spectroscopy we present the mathematical background of constructing the Fourier transform of a measured signal. Consider a one variable function, which is periodic from $[-\frac{T}{2}, \frac{T}{2}]$, the Fourier series of the function is:

$$\begin{aligned}
 h(t) &= \frac{a_0}{2} + \sum_{n=1}^{\infty} a_n \cos(n\omega_0 t) + b_n \sin(n\omega_0 t) \\
 a_n &= \frac{2}{T} \int_{-T/2}^{T/2} h(t) \cos(n\omega_0 t) dt \\
 b_n &= \frac{2}{T} \int_{-T/2}^{T/2} h(t) \sin(n\omega_0 t) dt
 \end{aligned} \tag{22}$$

where $\omega_0 = \frac{2\pi}{T}$.

For further convenience we turn to complex formalism. Using the Euler identity, we can rewrite Eq.(1) in the following form:

$$\begin{aligned}
 h(t) &= \sum_{n=-\infty}^{\infty} c_n e^{in\omega_0 t} : \\
 c_n &= \frac{2}{T} \int_{-T/2}^{T/2} h(t) e^{-in\omega_0 t} dt \\
 c_n &= \frac{1}{2} (a_n - ib_n) \\
 c_{-n} &= c_n^*
 \end{aligned} \tag{23}$$

In a more general way we can extend the previously showed calculation to a non periodic function by considering $T \rightarrow \infty$, this means that we have to include more harmonic functions, thus $n \rightarrow \infty$ $n\omega_0 \rightarrow \omega$. Under these conditions using that : $\sum \frac{1}{T} \rightarrow \int_{-\infty}^{\infty} df$, Eq.(2) yields the formulas of Fourier transformation:

$$\begin{aligned}
 H(\omega) &= \int_{-\infty}^{\infty} h(t) e^{i\omega t} dt \\
 h(t) &= \int_{-\infty}^{\infty} H(\omega) e^{-i\omega t} d\omega
 \end{aligned} \tag{24}$$

The meaning of the Fourier transform can be depicted as the follows: suppose we have a signal which is the superposition of harmonic functions, the Fourier transform shows what frequency components are present in the signal, as demonstrated by the following calculation:

Consider the function $h(t) = \cos(\omega_0 t)$, then using Euler's identity:

$$\begin{aligned}
 h(t) &= \frac{1}{2} (e^{i\omega_0 t} + e^{-i\omega_0 t}) \\
 H(\omega) &= \frac{1}{2} \delta(\omega - \omega_0) + \frac{1}{2} \delta(\omega + \omega_0)
 \end{aligned} \tag{25}$$

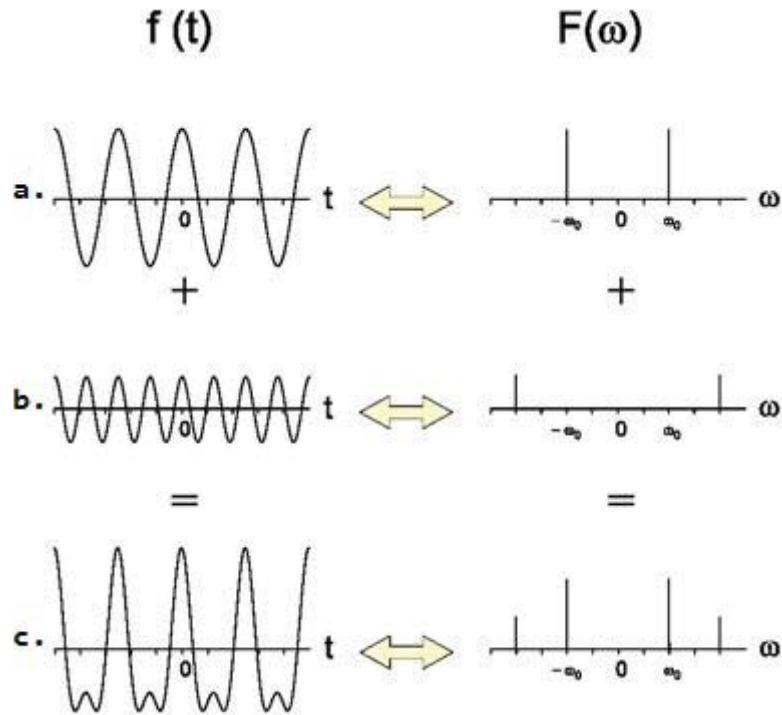


Figure 55: The functions in a. and b. are harmonics with different frequency and amplitude, beside them are their Fourier transform. Figure c. shows the superposition of the two functions, and the Fourier transform too

Consider the Fourier transform of a measured signal, which is neither continuous nor infinite in time for we measure in discrete points for a finite time (let us restrict our discussion to the measurement of periodical function). The basic concept is that we carry out a Fourier series like trigonometric polynomial interpolation, where the Fourier coefficients are calculated numerically, this method is called *Discrete Fourier Transformation* or *DFT*. Now suppose we have a continuous function $f(t)$ that we measure in the discrete t_k moments, where $k = 0, 1, \dots, n$, that means a total of $n + 1$ measurement points. Let us denote $f(t_k) = f_k$, now by intuition we suppose that an $m = \frac{n}{2}$ degree harmonic polynomial (Fourier series) will fit the measured points, that is we approximate our measured signal with:

$$h_m(t) = a_0 + \sum_{j=1}^m a_j \cos jt + b_j \sin jt \quad (26)$$

the a_0, \dots, a_m and b_0, \dots, b_m are called DFT coefficients. To calculate these coefficients a numerical integration is carried out on the Fourier integrals Eq.(1):

$$\begin{aligned} a_j &= \frac{1}{n+1} \sum_{k=0}^m f_k \cos jt_k \\ b_j &= \frac{1}{n+1} \sum_{k=0}^m f_k \sin jt_k \end{aligned} \quad (27)$$

One important property should be noticed from Eq.(5) that is: the maximum measurable frequency component in a signal sampled in n points is $m = \frac{n}{2}$, because as we can see the sum goes until $m = \frac{n}{2}$, that is if we want to measure a periodic signal with ω frequency, than we should sample with at least 2ω sampling frequency, this is the so-called *Nyquist criterium*.

When computing the *DFT* coefficients, the computer solves a Linear System of Equation using Eq.(5) and the function values f_k , which finally yields Eq. 6. Taking advantage of the properties of the matrix of *LSoE*, and if the number of measurement points is a power of 2, the number of calculations can be reduced dramatically, this technique is called *Fast Fourier Transformation*, and was introduced by James W. Cooley and W. Tukey in 1965. A detailed explanation can be found in [8]. Now days nearly every FT-spectrometer uses FFT algorithm to calculate the spectrum.

C The shot noise

If energy leaves a system eg. Raman photon emission, it will be carried by photons that will be emitted independently from each other, under such conditions the the number of emitted photons will follow Poisson process, and the probability of emission of N_{ph} photons during a Δt time, will be described by Poisson distribution :

$$P_{N_{ph}}(\Delta t) = \left(\frac{\Delta t}{\tau}\right)^{N_{ph}} \frac{1}{N_{ph}!} e^{-\Delta t/\tau} \quad (28)$$

$$\langle (N_{ph})^2 \rangle = \langle N_{ph} \rangle = \frac{\Delta t}{\tau}$$

Where τ is the average time between two emissions. The variance of Poisson distribution $\langle (N_{ph})^2 \rangle$ equals the expected value $\langle N_{ph} \rangle$.

As mentioned before, the number of the induced photo-electrons N_e is determined by the QE of the cathode material and is proportional with the number of incident photons, i.e. the cathode current of the PMT will also follows Poisson distribution, and the cathode current I_c will be

$$\langle I_c \rangle = \frac{\langle N_e \rangle e}{\Delta t}$$

$$\langle (\Delta I_c)^2 \rangle = \langle (\Delta N_e)^2 \rangle \frac{e^2}{(\Delta t)^2} = \langle \Delta N_e \rangle \frac{e^2}{(\Delta t)^2} \quad (29)$$

$$\langle (\Delta I_c)^2 \rangle = \langle I \rangle \frac{e}{\Delta t}$$

$$\langle (\Delta I_c)^2 \rangle = \langle I \rangle 2e\Delta f$$

where Δt now is the integration time, e is the elementary charge. In the last equation I used the Nyquist criterium that is $\Delta f = \frac{1}{2\Delta t}$, Eq. 29 shows that.

D The interferometer and other optical parts

Fig. 56 shows that the interferometer is insensitive to the AOI of the light at its entrance. The quality of the interferogram is determined by the relative alignment of the two mirrors with respect to one another. The solid line is the light path for optimal, perpendicular incidence on the mirrors. The two sets of dashed lines are diverted from the optimal alignment (shown exaggerated). Note that for both dashed lines, the light outputs from the two mirrors parallel to each other, which is a prerequisite for an interference. This shows that this type of interferometer is stable against small variations of the input light. It however does not tolerate even a small misalignment of the two mirrors against each other.

Fig. 57 shows a short, practical summary of parameters which affect the spectrometer performance. A classification is given which are the sensitive and non-sensitive parameters.

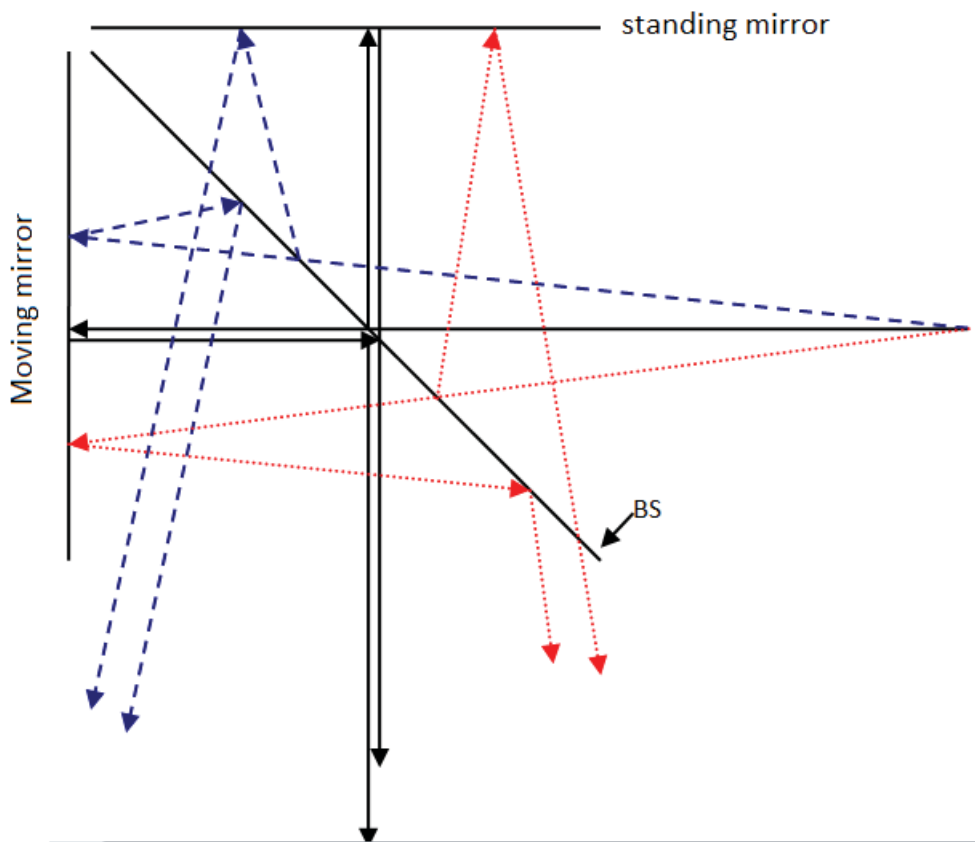


Figure 56: The interferogram independence of the entering beam AOI

	sensitive	not sensitive	comment
Laser screw	x		
focusing lens 90° geomtery			if 90° geomtery is desired it must be applied
Orintation (small) mirror	x		very sensitive
position of the sample		x	must be located in the focus
parabolic mirror		x	not sensitive in a given range
edge filter		x	not sensitive in a given range
beamsplitter	x		
steady mirror	x		
detector's parabolic mirror		x	not sensitive in a given range

Figure 57: Table of the sensitivity of different optical paths in *Bruker IFS66v* spectrometer

E Applied HAMAMATSU PMT datasheet

Extended Red, High Sensitivity, Multialkali Photocathode 28 mm (1-1/8 Inch) Diameter, 9-Stage, Side-On Type

The R928 and R955 feature extremely high quantum efficiency, high current amplification, good S/N ratio and wide spectral response from UV to near infrared. The R928 employs a UV glass envelope and the R955 has a fused silica envelope for UV sensitivity extension. The R928 and R955 are well suited for use in broad-band spectrophotometers, atomic absorption spectrophotometers, emission spectrophotometers and other precision photometric instruments.

FEATURES

- Wide Spectral Response
 - R928 185 nm to 900 nm
 - R955 160 nm to 900 nm
- High Cathode Sensitivity
 - Luminous 250 $\mu\text{A/lm}$
 - Radiant at 400 nm 74 mA/W
- High Anode Sensitivity (at 1000 V)
 - Luminous 2500 A/lm
 - Radiant at 400 nm $7.4 \times 10^5 \text{ A/W}$
- Low Drift and Hysteresis

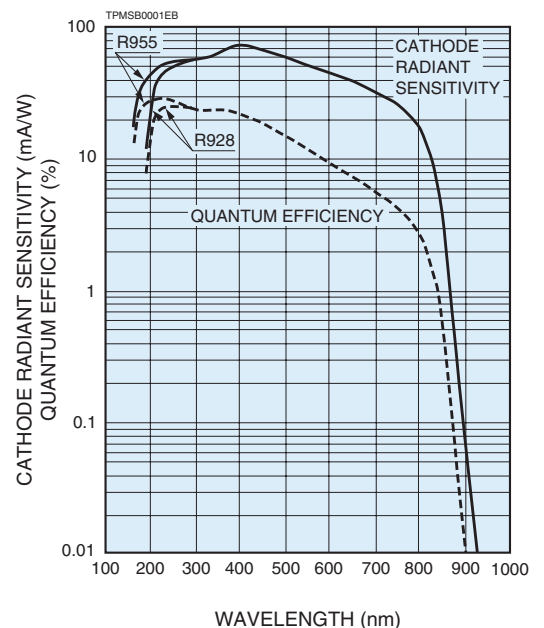


SPECIFICATIONS

GENERAL

Parameter		Description/Value	Unit
Spectral Response	R928	185 to 900	nm
	R955	160 to 900	nm
Wavelength of Maximum Response		400	nm
Photocathode	Material	Multialkali	—
	Minimum Effective Area	8×24	mm
Window Material	R928	UV glass	—
	R955	Fused silica	—
Dynode	Secondary Emitting Surface	Multialkali	—
	Structure	Circular-cage	—
	Number of Stages	9	—
Direct Interelectrode Capacitances	Anode to Last Dynode	4	pF
	Anode to All Other Electrodes	6	pF
Base		11-pin base JEDEC No. B11-88	—
Weight		Approx. 45	g
Operating Ambient Temperature		-30 to +50	$^{\circ}\text{C}$
Storage Temperature		-30 to +50	$^{\circ}\text{C}$
Suitable Socket		E678-11A (Sold Separately)	—
Suitable Socket Assembly		E717-63 (Sold Separately)	—
		E717-74 (Sold Separately)	—

Figure 1: Typical Spectral Response



PHOTOMULTIPLIER TUBES R928, R955

MAXIMUM RATINGS (Absolute Maximum Values)

Parameter		Value	Unit
Supply Voltage	Between Anode and Cathode	1250	V
	Between Anode and Last Dynode	250	V
Average Anode Current ^A		0.1	mA

CHARACTERISTICS (at 25 °C)

Parameter		R928			R955			Unit	
		Min.	Typ.	Max.	Min.	Typ.	Max.		
Cathode Sensitivity	Quantum Efficiency (at Peak Wavelength)	—	25.4 (at 260 nm)	—	—	29.0 (at 220 nm)	—	%	
	Luminous ^B	140	250	—	140	250	—	μA/lm	
	Radiant	at 194 nm	—	18	—	—	43	—	mA/W
		at 254 nm	—	52	—	—	56	—	mA/W
		at 400 nm	—	74	—	—	74	—	mA/W
		at 633 nm	—	41	—	—	41	—	mA/W
		at 852 nm	—	3.5	—	—	3.5	—	mA/W
Red/White Ratio ^C	0.2	0.3	—	0.2	0.3	—	—		
Blue Sensitivity Index ^D	—	8	—	—	8	—	—		
Anode Sensitivity	Luminous ^E	400	2500	—	400	2500	—	A/lm	
	Radiant	at 194 nm	—	1.8 × 10 ⁵	—	—	4.3 × 10 ⁵	—	A/W
		at 254 nm	—	5.2 × 10 ⁵	—	—	5.6 × 10 ⁵	—	A/W
		at 400 nm	—	7.4 × 10 ⁵	—	—	7.4 × 10 ⁵	—	A/W
		at 633 nm	—	4.1 × 10 ⁵	—	—	4.1 × 10 ⁵	—	A/W
		at 852 nm	—	3.5 × 10 ⁴	—	—	3.5 × 10 ⁴	—	A/W
Gain ^E	—	1.0 × 10 ⁷	—	—	1.0 × 10 ⁷	—	—		
Anode Dark Current ^F (After 30 min Storage in Darkness)		—	3	50	—	3	50	nA	
ENI (Equivalent Noise Input) ^H		—	1.3 × 10 ⁻¹⁶	—	—	1.3 × 10 ⁻¹⁶	—	W	
Time Response ^E	Anode Pulse Rise Time ^I	—	2.2	—	—	2.2	—	ns	
	Electron Transit Time ^J	—	22	—	—	22	—	ns	
	Transit Time Spread (TTS) ^K	—	1.2	—	—	1.2	—	ns	
Anode Current Stability ^L	Light Hysteresis	—	0.1	—	—	0.1	—	%	
	Voltage Hysteresis	—	1.0	—	—	1.0	—	%	

NOTES

- A: Averaged over any interval of 30 seconds maximum.
 B: The light source is a tungsten filament lamp operated at a distribution temperature of 2856K. Supply voltage is 100 V between the cathode and all other electrodes connected together as anode.
 C: Red/White ratio is the quotient of the cathode current measured using a red filter (Toshiba R-68) interposed between the light source and the tube by the cathode current measured with the filter removed under the same conditions as Note B.
 D: The value is cathode output current when a blue filter (Corning CS 5-58 polished to 1/2 stock thickness) is interposed between the light source and the tube under the same condition as Note B.
 E: Measured with the same light source as Note B and with the voltage distribution ratio shown in Table 1 below.

Table 1: Voltage Distribution Ratio

Electrode	K	Dy1	Dy2	Dy3	Dy4	Dy5	Dy6	Dy7	Dy8	Dy9	P
Distribution Ratio	1	1	1	1	1	1	1	1	1	1	1

Supply Voltage: 1000 V, K: Cathode, Dy: Dynode, P: Anode

- F: Measured with the same supply voltage and voltage distribution ratio as Note E after removal of light.
 G: Measured at a supply voltage adjusted to provide an anode sensitivity of 100 A/lm.

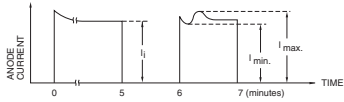
- H: ENI is an indication of the photon-limited signal-to-noise ratio. It refers to the amount of light in watts to produce a signal-to-noise ratio of unity in the output of a photomultiplier tube.

$$ENI = \frac{\sqrt{2q \cdot I_{db} \cdot G \cdot \Delta f}}{S}$$

- where q = Electronic charge (1.60 × 10⁻¹⁹ coulomb).
 I_{db} = Anode dark current (after 30 minute storage) in amperes.
 G = Gain.
 Δf = Bandwidth of the system in hertz. 1 hertz is used.
 S = Anode radiant sensitivity in amperes per watt at the wavelength of peak response.

- I: The rise time is the time for the output pulse to rise from 10 % to 90 % of the peak amplitude when the entire photocathode is illuminated by a delta function light pulse.
 J: The electron transit time is the interval between the arrival of delta function light pulse at the entrance window of the tube and the time when the anode output reaches the peak amplitude. In measurement, the whole photocathode is illuminated.
 K: Also called transit time jitter. This is the fluctuation in electron transit time between individual pulses in the signal photoelectron mode, and may be defined as the FWHM of the frequency distribution of electron transit times.

L: Hysteresis is temporary instability in anode current after light and voltage are applied.



TPMSB0002EA

$$\text{Hysteresis} = \frac{I_{\text{max}} - I_{\text{min}}}{I_i} \times 100 (\%)$$

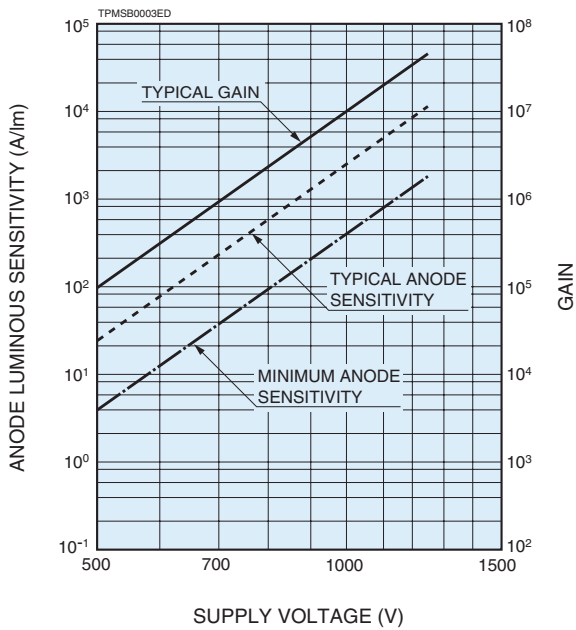
(1) Light Hysteresis

The tube is operated at 750 V with an anode current of 1 μA for 5 minutes. The light is then removed from the tube for a minute. The tube is then re-illuminated by the previous light level for a minute to measure the variation.

(2) Voltage Hysteresis

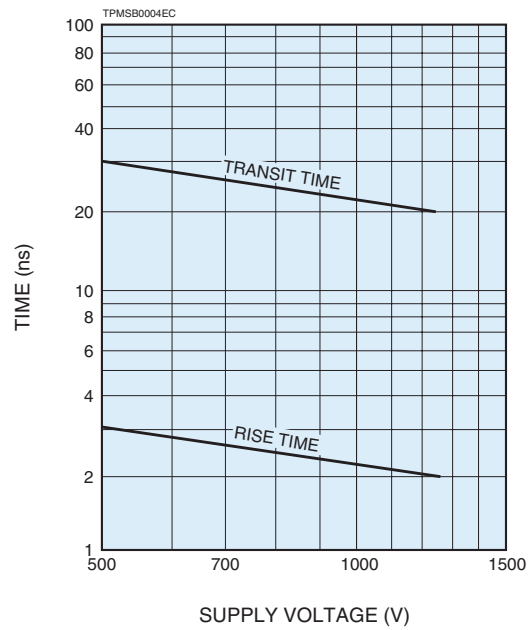
The tube is operated at 300 V with an anode current of 0.1 μA for 5 minutes. The light is then removed from the tube and the supply voltage is quickly increased to 800 V. After a minute, the supply voltage is then reduced to the previous value and the tube is re-illuminated for a minute to measure the variation.

Figure 2: Anode Luminous Sensitivity and Gain Characteristics



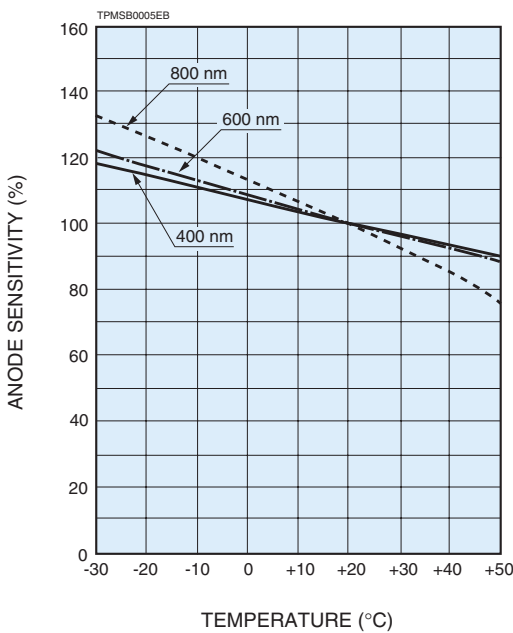
TPMSB0003ED

Figure 3: Typical Time Response



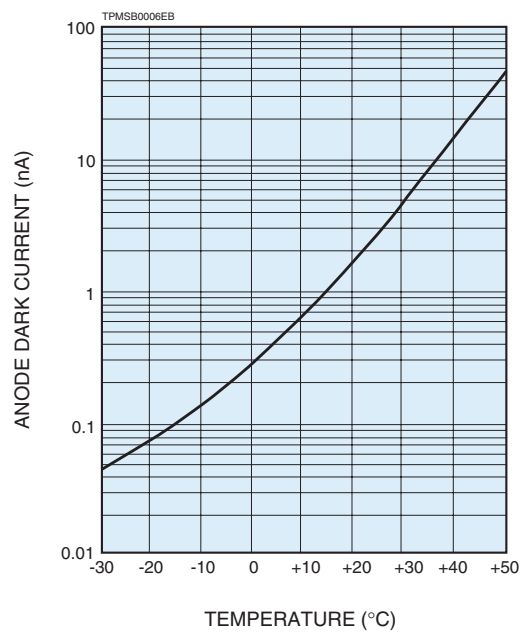
TPMSB0004EC

Figure 4: Typical Temperature Coefficient of Anode Sensitivity



TPMSB0005EB

Figure 5: Typical Temperature Characteristic of Dark Current (at 1000 V, after 30 min storage in darkness)



TPMSB0006EB